Biomimatic material(생체 모방 재료)의 나노 구조 및 조립에 대한 연구 동향

Chung-Ang University, Da Vinci College of General Education
OK JA Yoon

CHERIC
Chemical Engineering and Materials Research Information Center
국가지정
화학공학소재연구정보센터

연구 동향

✓ **Biomimetic fabrication of micro-/nanostructure on polypropylene surfaces with high dynamic superhydrophobic stability[1]**

- Huang et al.은 무전해 도금 (electroless plating)과 전기 도금 (electroplating)을 이용하여 연잎 (lotus leaf)의 nickel template를 제작하였고, PP(polypropylene) 를 이용하여 연잎의 micro-/nano-structure를 재현하였음.

- 제작 과정은 간단하여 산업적으로 적용 가능하고 대량생산이 가능한 기술임. 니켈 복제물(nickel replica)은 연잎에 무전해 도금과 전기 도금을 하여 제조된 자연 주형임. 제조된 니켈 템플레이트(nickel template)를 사용한 사출 성형 (injection molding)에 의해 PP 표면에 연잎 형태의 구조가 만들어짐.

- 제작된 PP 복제물 (replica)은 연잎의 마이크로 구조 (micro structure)를 성공적으로 재현하였고, 나노 구조 (nano structure)의 경우, 연잎의 nanotube의 형태를 가진 nanohair 형태를 띠고 있음. 높은 종횡 비 (high aspect ratio)와 날카로운 tip 형태를 가진 nanohair는 추가적인 표면 코팅이나 화학적 개질 없이 구조를 만들어 연잎의 micro-/nano-structure를 모방하여 제작함.

- PP 복제물의 표면은 4-μL droplet에 대해서 contact angle 157 ± 2°, run-off angle가 5°이하, CA hysteresis 5 ± 4°이며, "contacting-compressing-releasing" test에서는 물방울이 구의 형태를 유지하면서 water adhesion이 관찰되지 않는 특징을 확인함.

- 100 ℃의 물에 연잎과 PP 복제물을 넣었을 때, 연잎은 1분만에 접촉각(cantact angle)이 159°에서 112°로 감소하였으나, PP 복제물은 157°에서 152°로 감소하여 고온에서 연잎보다 더 잘 견디는 모습을 확인함. droplet impact test에서는 물방울이 impact-rebound까지 걸리는 시간이 PP 복제물이 8ms로 연잎에 비해 3ms적게 걸리면서 PP 복제물의 nanohair 구조가 thermal durability와 dynamic super-hydrophobic stability 측면에서 우월한 특성을 보여주었음.

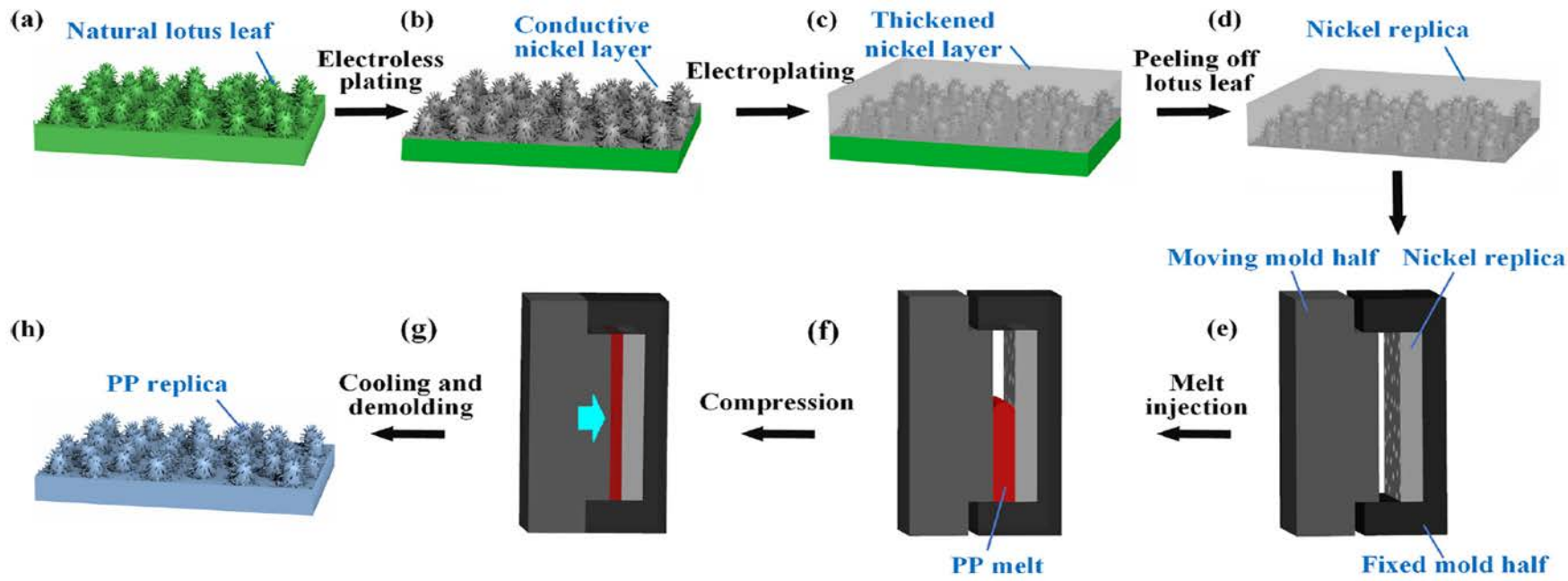

Fig. 1. Schematics of fabrication process for biomimetic PP replica with lotus leaf-like micro-/nanostructure. (a) 3D model of natural lotus leaf, (b) conductive layer deposition, (c) nickel deposition on conductive layer surface, (d) nickel replica, (e, f, g) μ-ICM process and (h) final PP replica.

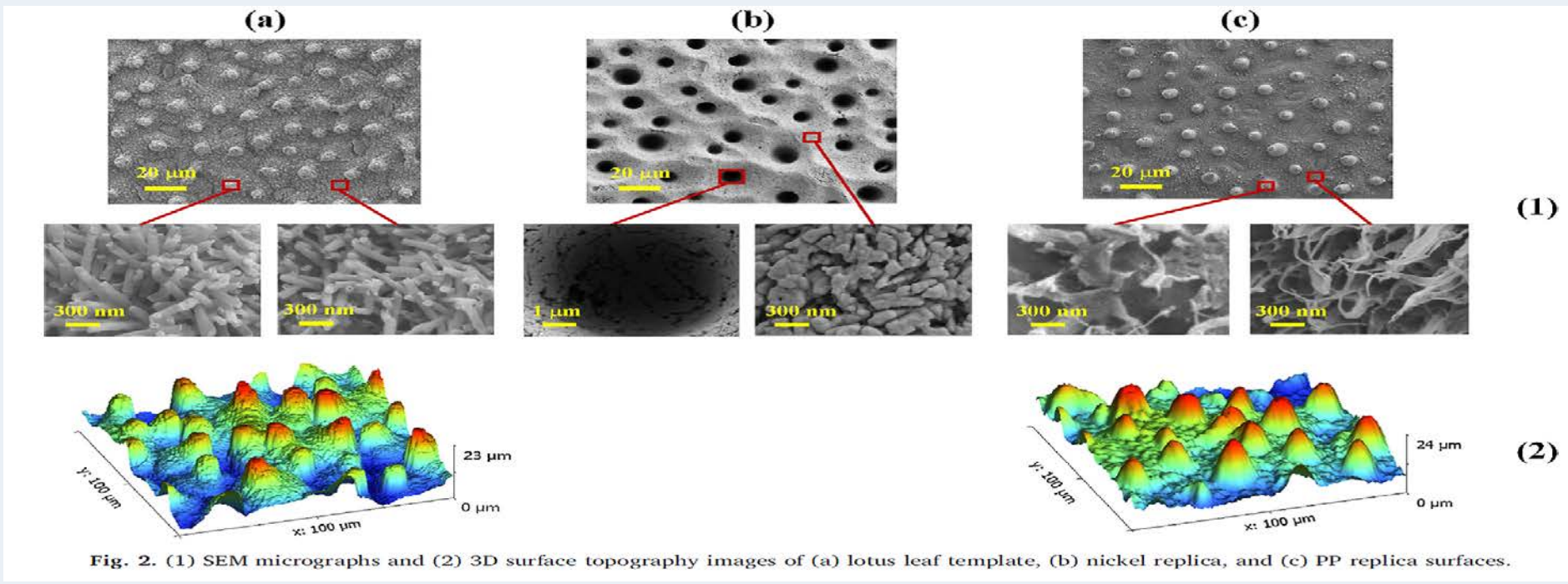

Fig. 2. (1) SEM micrographs and (2) 3D surface topography images of (a) lotus leaf template, (b) nickel replica, and (c) PP replica surfaces.

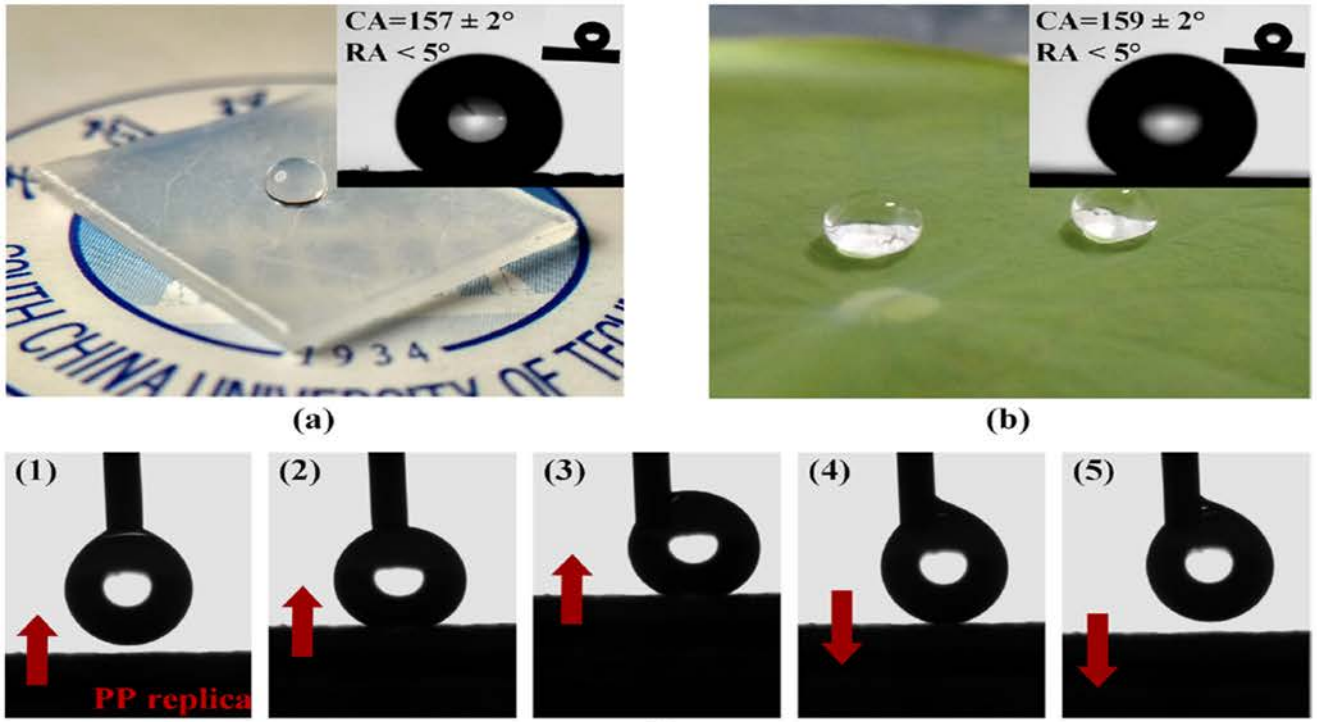

Fig. 3. Digital images of water droplets placed on (a) PP replica and (b) lotus leaf surfaces (Insets show wetting state of 4-μL water droplets); (c) representative snapshots of water droplet (4 μL) (1) suspending on needle, (2) slightly and (3) tightly contacted with lifting PP replica surface and (4, 5) departing from lowering surface (Arrows represent moving direction of PP replica).

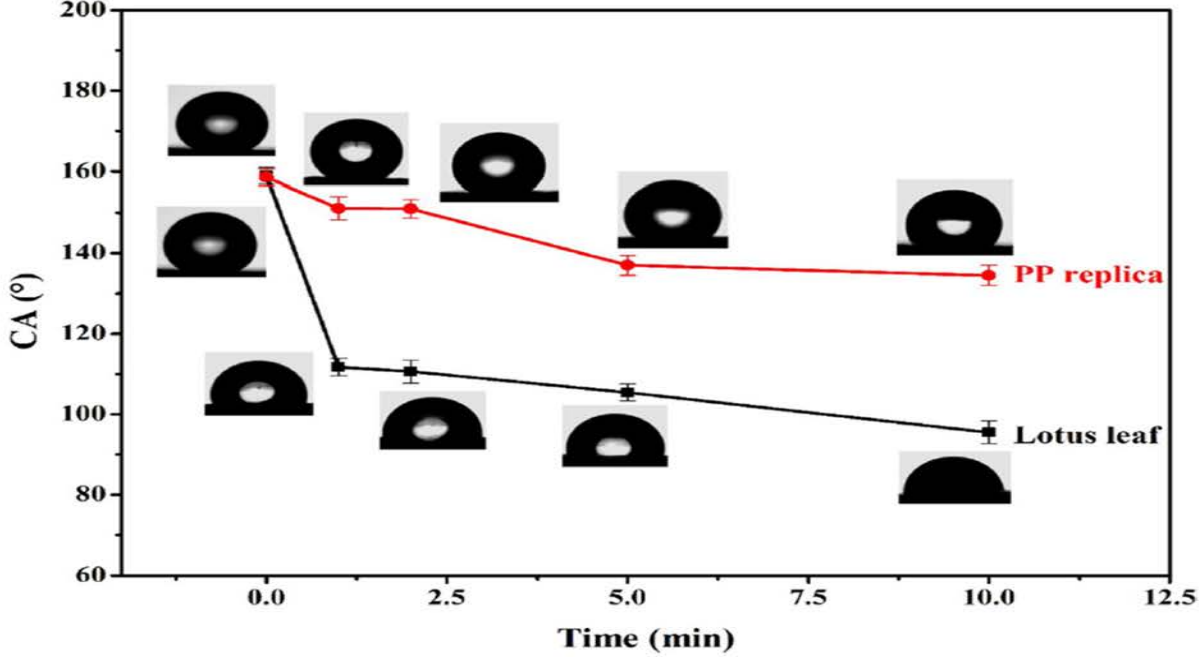

Fig. 4. Contact angle on thermally annealed lotus leaf and PP replica versus thermal annealing time curves. Insets show wetting state of droplets.

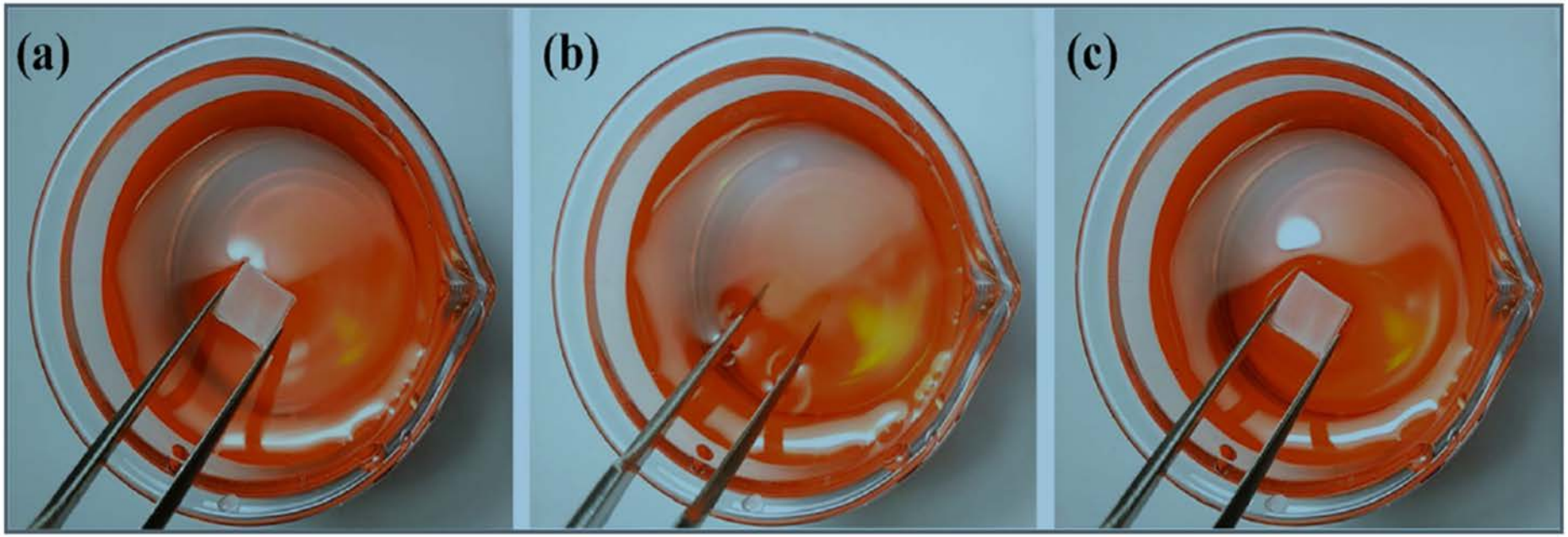

Fig. 5. Typical snapshots of PP replica (a) before, (b) during, and (c) after being immersed in methyl red-dyed water.

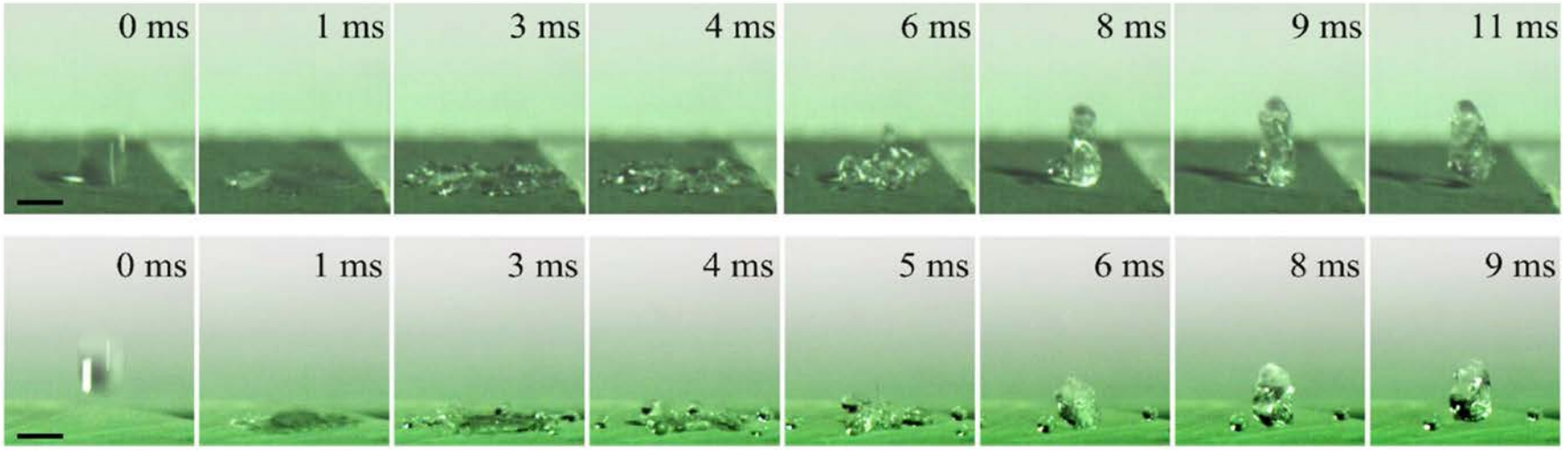

Fig. 6. Time sequence images of droplet (~3 mm in diameter) free falling on (a) lotus leaf and (b) PP replica surfaces (Impact velocity: 1.98 m/s; Scale bar: 2 mm).

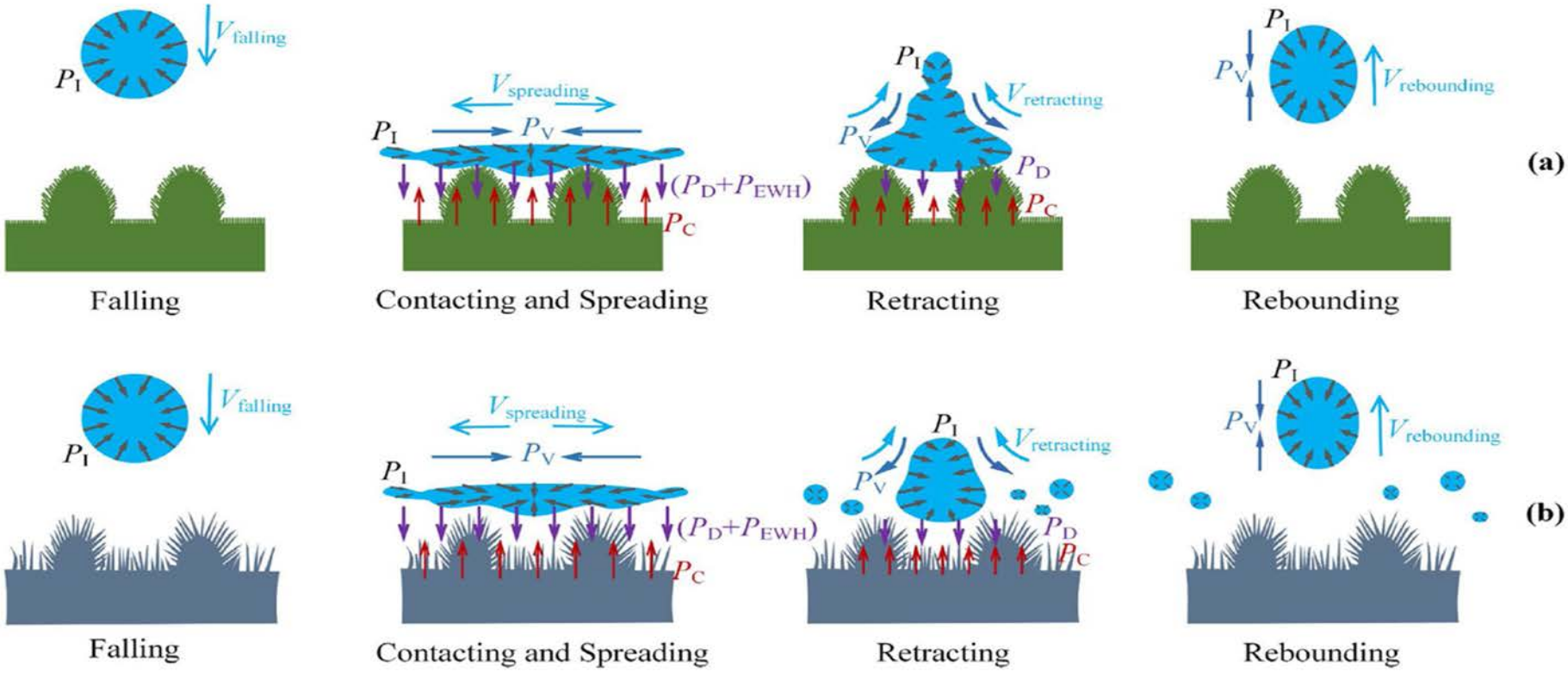

Fig. 8. Underlying mechanism of droplet impact dynamics on (a) lotus leaf and (b) PP replica.

✓ Biomimetic Nanostructure Fabrication to Increase Light Transmission Efficiency in Optoelectronic Devices[2]

- 발광 다이오드 (light emitting diode)와 포토 다이오드 쌍 (photodiode pair)의 광전자 장치 (optoelectronic devices)에 생체 모방 서브 파장 나노 구조 (biomimetic sub-wavelength nanostructures)를 제조함으로써 두 장치 사이의 커플링을 향상시키는 것에 대한 연구를 보고함.

- 제조 과정은 Si substrate 위에 PS nanosphere를 주기적으로 배치시키고, 여러 단계의 reactive ion etching(RIE)와 실란화 (silanization)를 거쳐 moth-eye 와 같은 나노 구조 (nano structure) 를 형성시켰고, polydimethylsiloxane(PDMS)로 나노 임프린팅 (nano imprinting)을 위한 몰드 (mold)를 만들었음. UV resin과 PDMS mold로 구현한 moth-eye와 같은 구조는 너비 151nm, 높이가 358nm인 돌기가 198nm의 주기로 규칙적인 배열이 형성됨.

- Inorganic light emitting diode와 photodiode 장치 표면에 형성된 생체 모방 나노 구조를 붙인 후 optical device pair의 photodiode 출력을 측정한 결과, 붙이지 않은 경우에 비해 Photodiode에 흐르는 Mean Current가 21.4% 증가하였음. 반대로 flat UV resin을 붙인 결과, Mean Current가 7.7% 감소하는 결과를 보여주었음.

- 이러한 결과는 발광기와 검출기 한 쌍을 사용하는 감지 시스템 응용이 유망함.

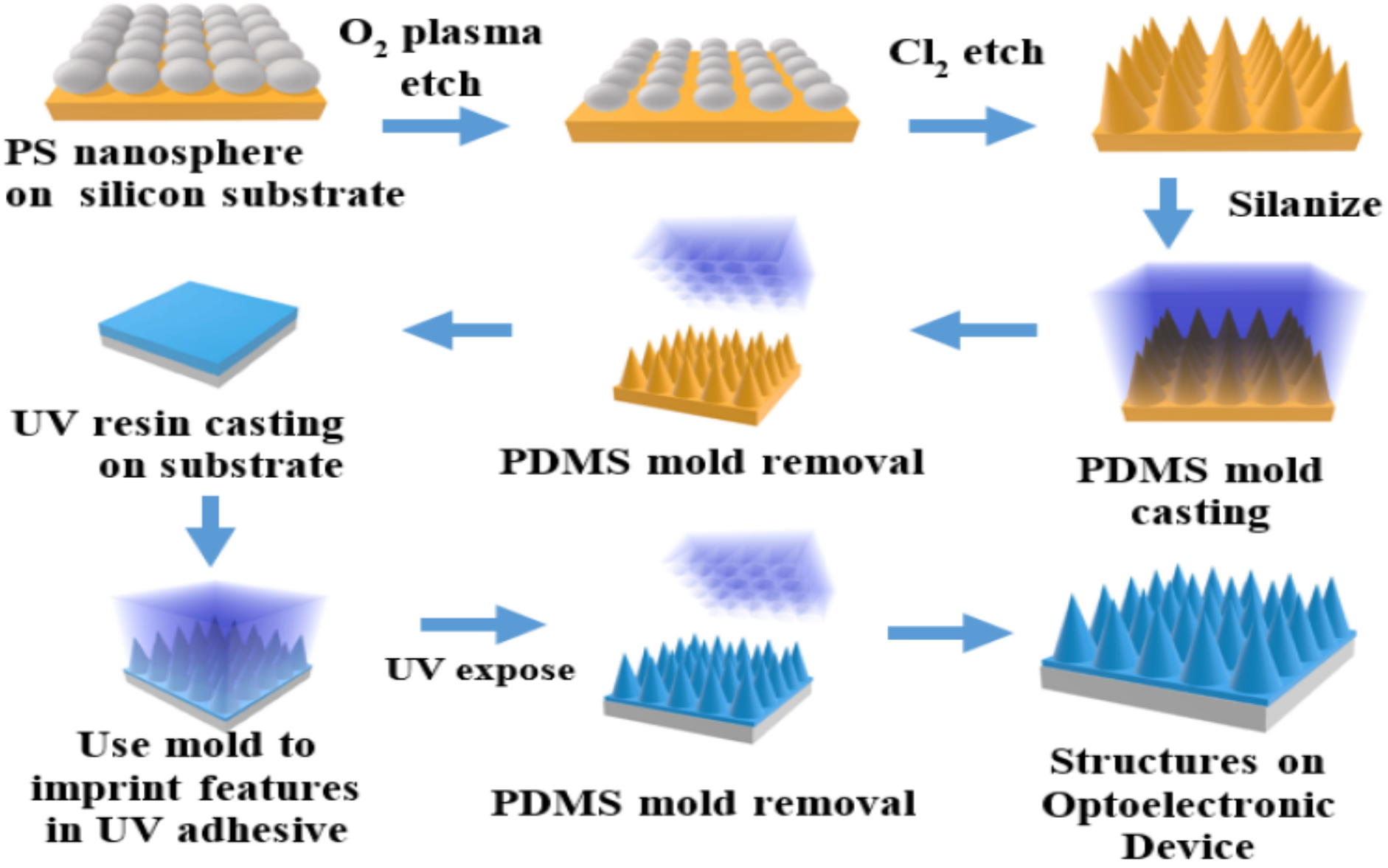

Figure 1. Steps to fabricate the moth-eye like structure include a polystyrene (PS) mask deposition on silicon, reactive ion etching (RIE), mold making, and stamping the pattern into UV curable adhesive on an optoelectronic device.

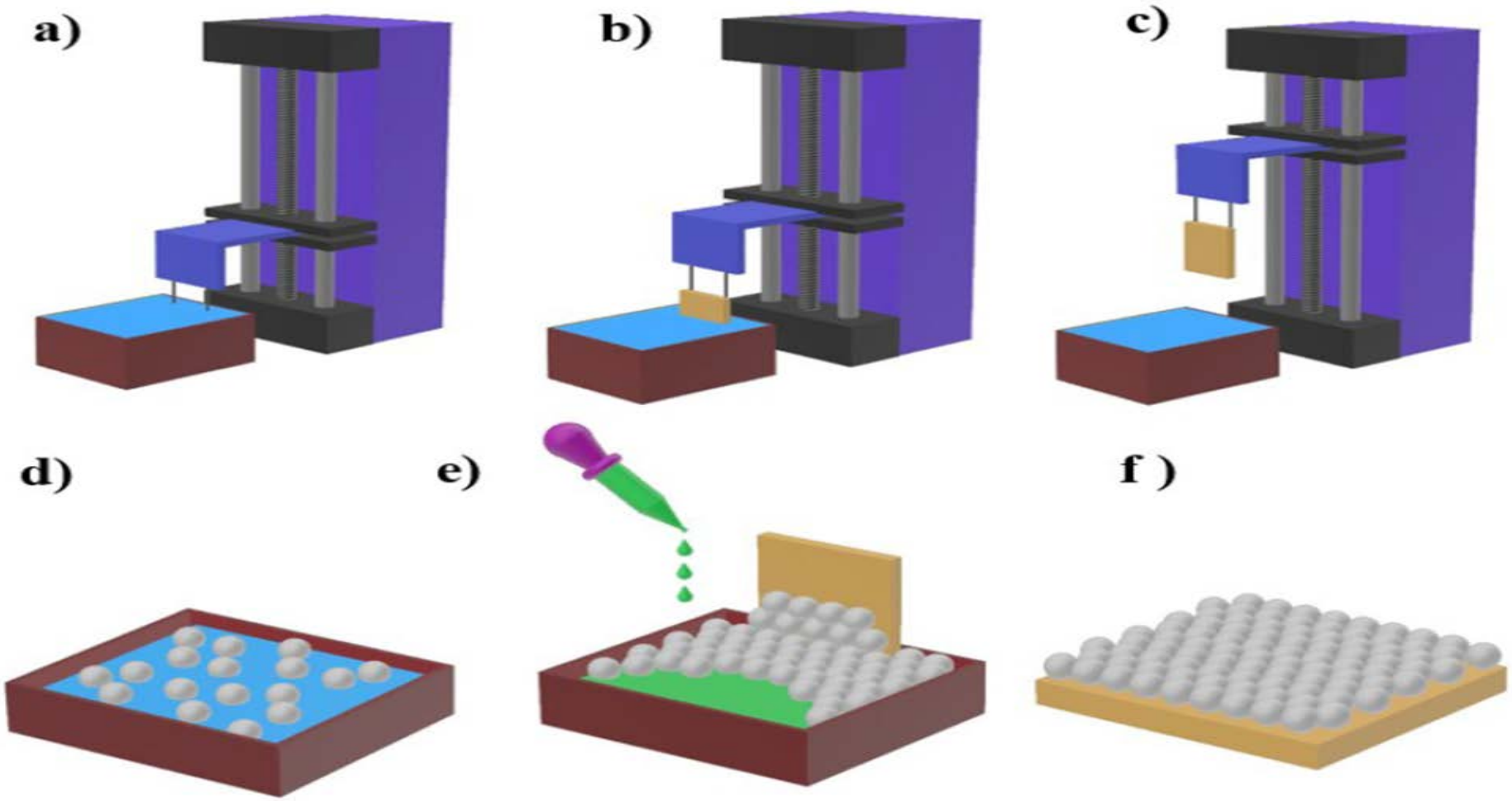

Figure 2. A schematic illustration showing the syringe pump with the cantilever arm slowly lifting the silicon substrate out of the water with the polystyrene nanosphere monolayer. d) The nanospheres are initially distributed across the water surface in an unordered monolayer. e) A dropper introduces a 5% solution of sodium dodecyl sulfate (SDS) that compacts the monolayer to form a highly ordered colloidal crystal that is deposited on the silicon while it is withdrawn from the water. f) The silicon becomes covered with the polystyrene nanosphere monolayer and set aside to dry.

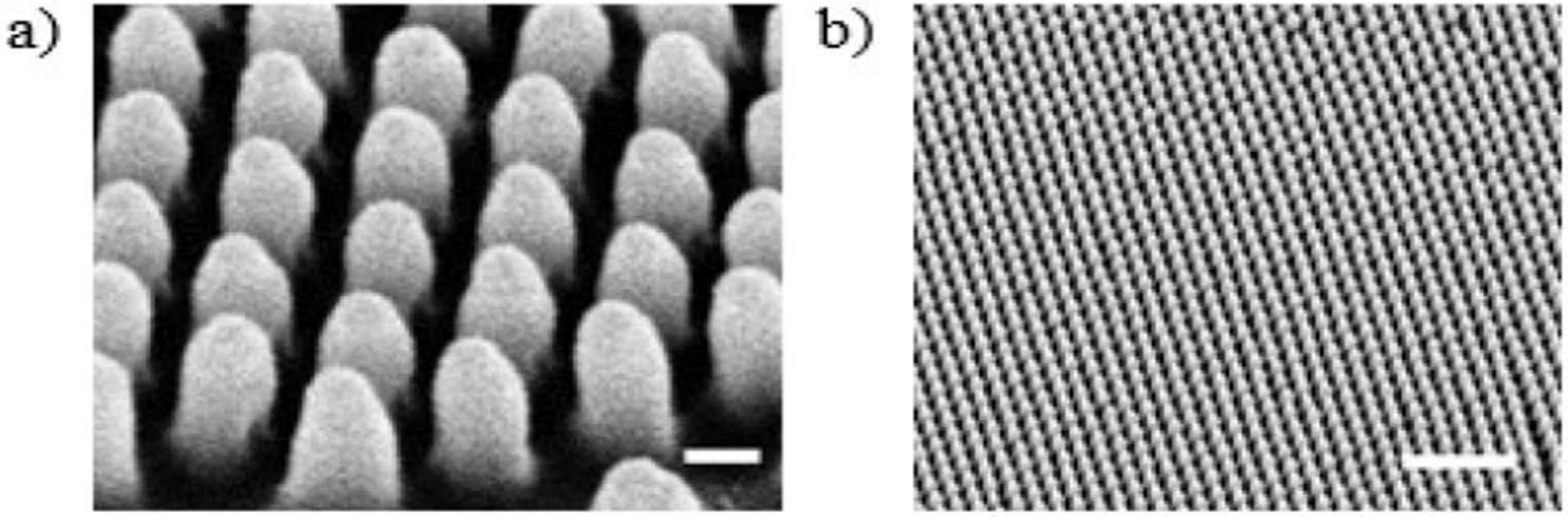

Figure 3. Examples of the a) biomimetic moth-eye nanostructures (scale bar 100 nm) and b) their long range order (scale bar 1 micron) as fabricated in optical adhesive.

TABLE 1: NANOSTRUCTURE MEASUREMENTS

	N	Mean (nm)	Standard Dev.
Height	84	356	17.6
Width	17	151	10.3
Period	14	198	5.1

TABLE 2: COUPLING RESULTS UNDER DIFFERENT CONDITIONS

Pair Type	N (device pairs)	Photodiode (PD) Mean Current (nA)	Standard Dev.	Percent Difference Relative to Bare Device Pair
Bare LED/PD	3	15.9	0.3	-
Flat Glue on LED/PD	2	14.6	-	-7.7%
Moth-Eye Patterned on LED/PD	3	19.3	3.5	+21.4%

✓ Biomimicry of multifunctional nanostructures in the neck feathers of mallard (Anas platyrhynchos L.) drakes[3]

- 생물학적 시스템은 인공적으로 생체 모방하기 위한 기본적인 영감의 원천이며, 기존의 기술 개발은 복잡성, 생산선, 재료, 경제적인 면에서 아직은 기술이 미비함.

- Anas platyrhynchos drakes의 무지개 빛깔의 목 깃털 (neck feathers)은 hexagonally distributed melanin rods가 keratin에 둘러 쌓여있는 구조로, 좁은 영역의 wavelength에 해당하는 빛을 반사시키며, 이는 보는 각도에 따라 달라짐.

- iterative size reduction 방식 (연속적으로 크기를 감소시키는 방식)을 사용하여, Polycarbonate(PC) rod에 polyvinyldifluoride(PVDF) 와 PC를 번갈아 코팅한 nano wire를 polymer sheath에 넣어 photonic 2D crystal fiber를 제조함. photonic 2D crystal fiber은 neck feathers와 유사하게 각도에 따라 반사되는 빛의 파장이 달라지며, 녹색 fiber에 대하여 unpolarized light simulation과 측정결과가 일치하는 결과를 보여줌.

- Structure parameters (격자상수(Lattice constants), rod diameters)에 따라 색이 달라지며, band-structure calculations map으로 원하는 색의 fiber를 디자인 하는 것도 가능함. 또한, Neck feathers와 photonic 2D crystal fibers는 유사한 구조에 의해서 접촉각 (contact angle)이 최대 160°로 초 소수성 (super-hydrophobic) 특성을 보여줌.

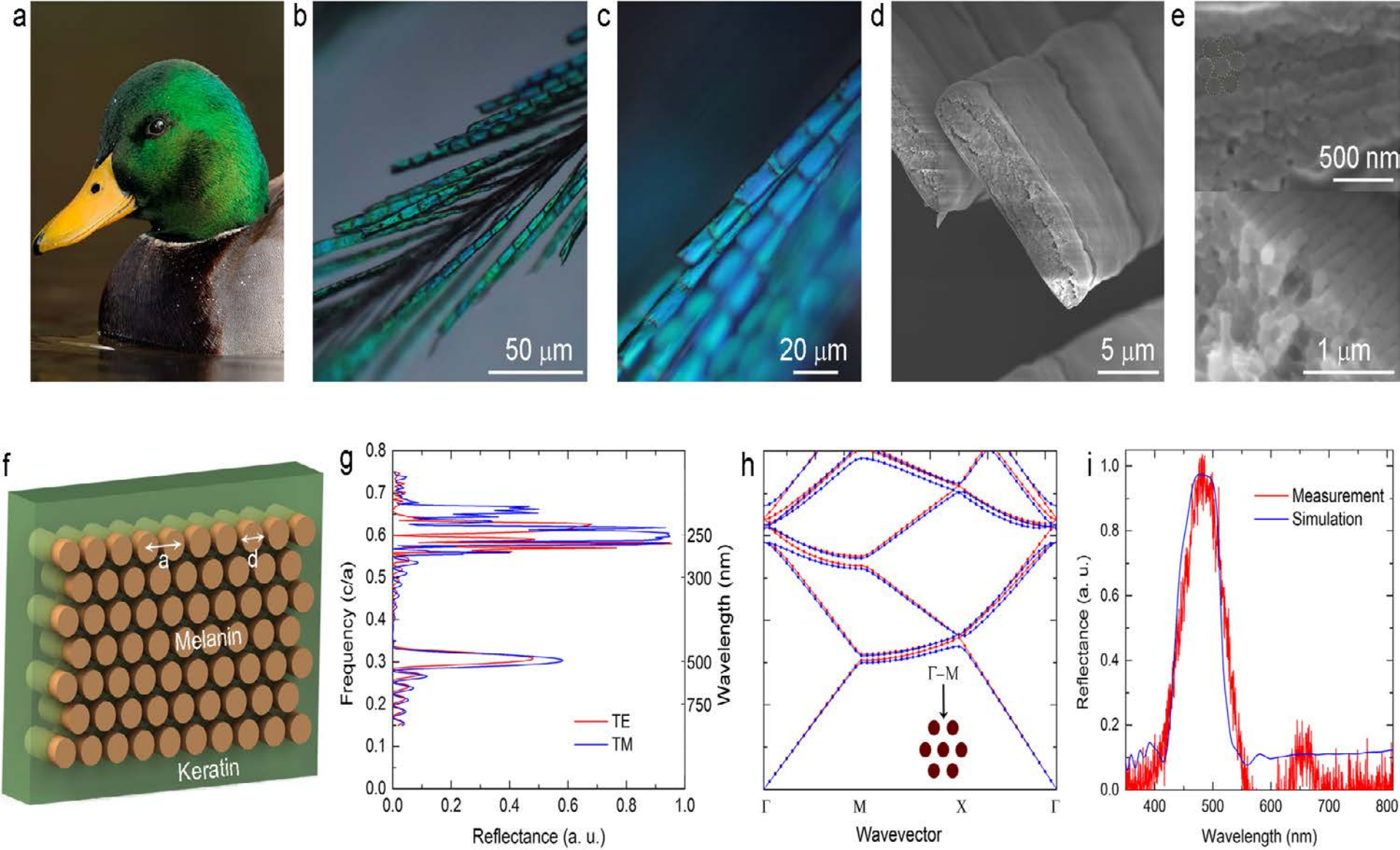

Figure 1 | Investigation of *A. platyrhynchos* feathers. (a), Mallard neck feathers are investigated for their structural properties (Photographed by Jacob S. Spendelow). Optical microscopy images of mallard neck feathers reveal that higher magnifications result in a change of coloration from (b), green to (c), blue, which suggests the presence of iridescence. Hexagonal arrays of rods are observed from (d), longitudinal and (e), cross-sectional SEM images of feather barbules to be distributed throughout the barbule periphery. (f), Scheme representing the distribution of melanin rods embedded in the keratin matrix. The associated lattice constants (a) and diameters (d) are observed to be around 150 nm and 130 nm, respectively. (g), Reflection simulation of neck feather barbules is performed using the above-mentioned values. (h), Band structure calculations show that directional band-gaps exist in the green and UV regions of the spectrum. (i), Experimental and simulation results associated with the optical features of mallard feathers are in good agreement.

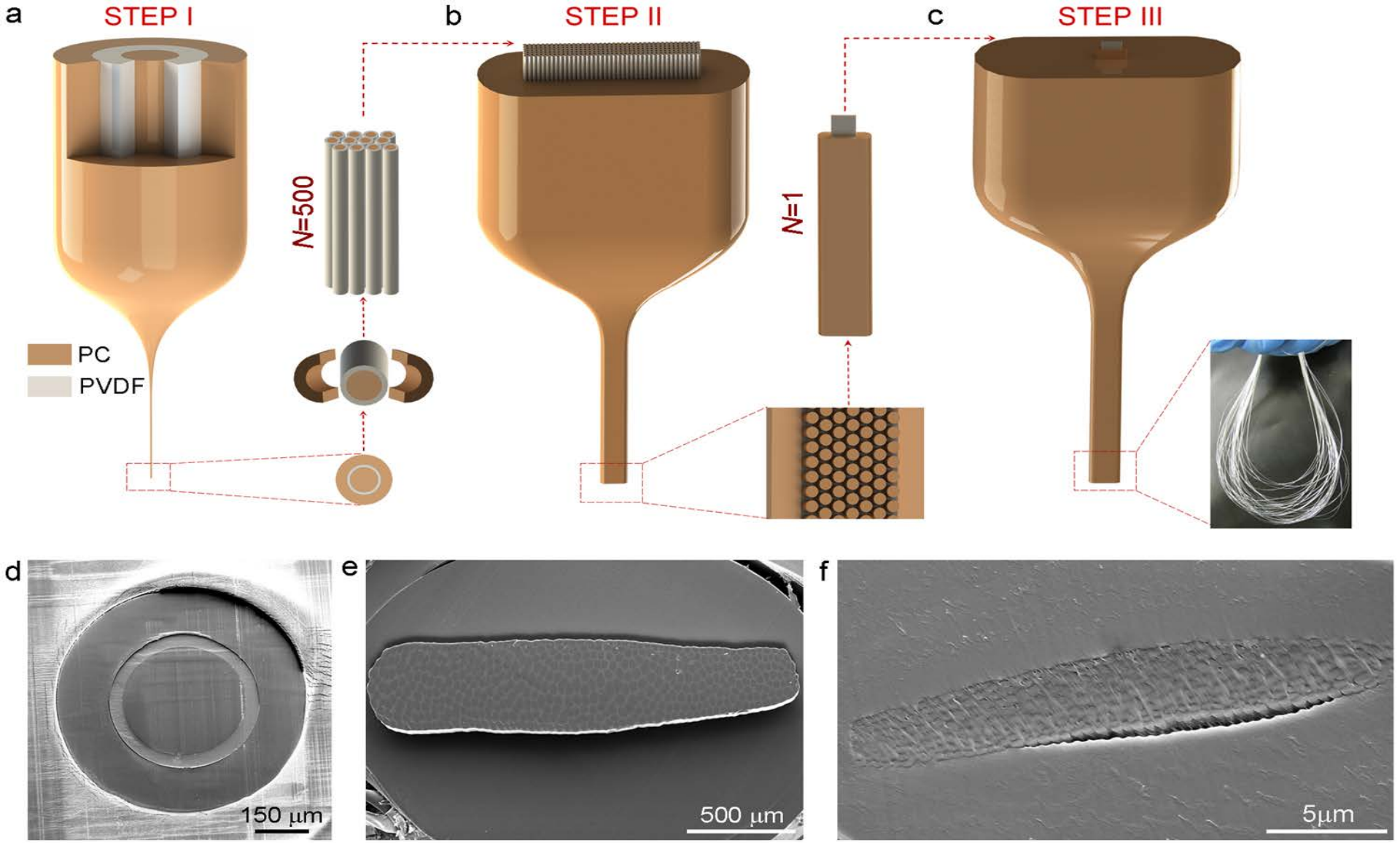

Figure 2 | Functional biomimetics of mallard drake feathers. A low temperature, multimaterial fibre drawing method is used for the iterative reduction of a macroscopic preform down to microscale photonic crystal. (a), The first step preform is obtained by successively wrapping PVDF and PC polymer films around a PC rod. The outer layer of step I fibres removed prior to the second step of fabrication. (b), In the second step, a rectangular formation is used in order to increase the aspect ratio of the final result, so as to resemble the design observed in *A. platyrhynchos* feathers. PVDF embedded PC microwires with lattice constants of several microns are produced at the end of step II. (c), Step III is performed by repeating previous fabrication procedures, and permits the precise control of the lattice constant in the 100-300 nm region. (d–f), Cross-sectional SEM images of produced fibers after steps I, II and III, respectively.

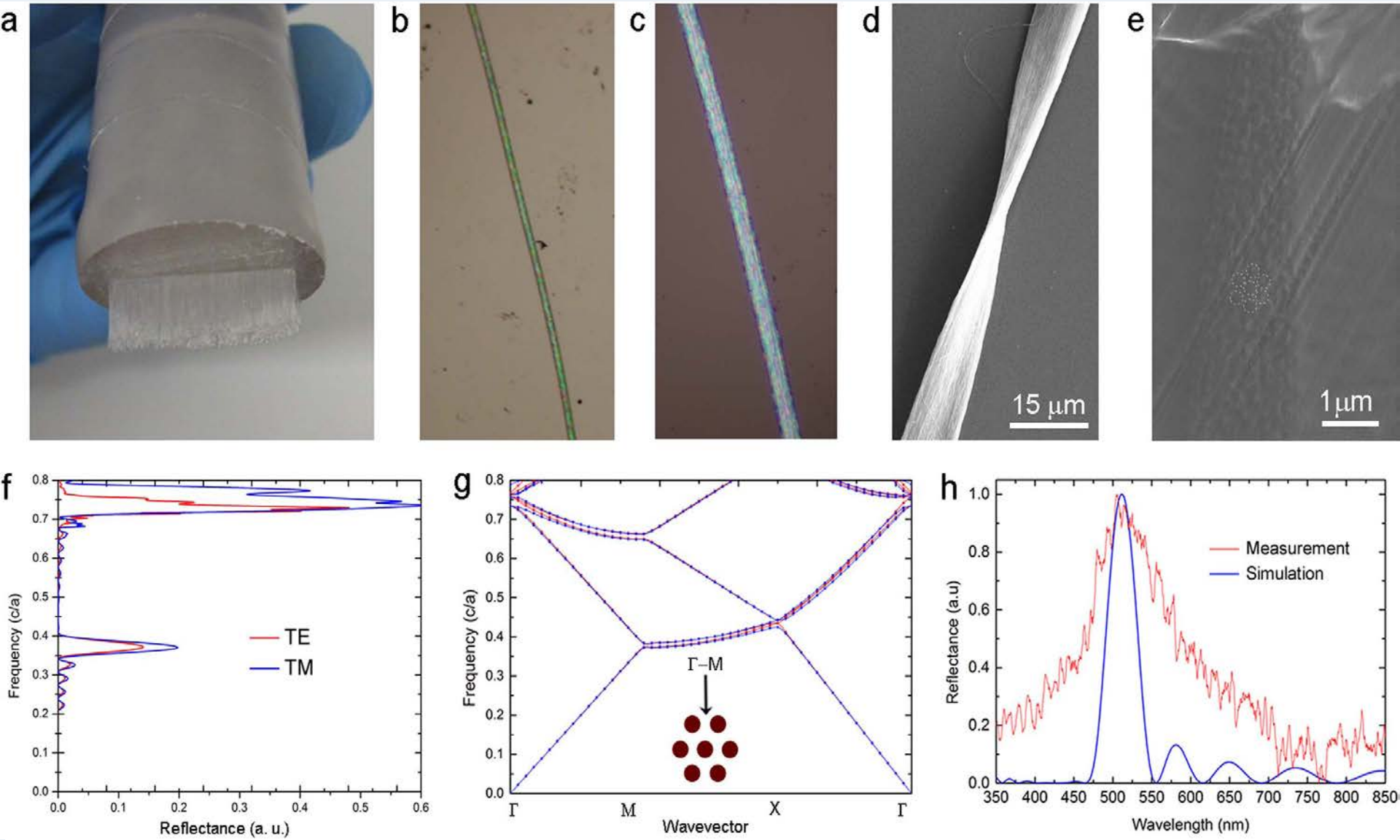

Figure 3 | Characterization of biomimetic all-polymer photonic crystal structures. (a), A diverse array of 2D photonic crystal nanostructures can be engineered from a unique macroscale preform. (b), The vivid green hue observed under light microcopy confirms the presence of photonic crystal effects. (c), Biomimetic photonic crystal fibres appear iridescent as the magnification of light microscope is increased. The green color is transformed into blue as a result of the photonic crystal effect. (d–e), SEM images reveal the ribbonlike photonic crystal formation and hexagonal distribution of PC rods inside the PVDF matrix, with lattice constants around 200 nm. (f), Reflection and (g), bandstructure calculations are performed using the optical and size parameters of the material components. (h), Reflection measurements from green colored photonic crystal structures are consistent with FDTD modelling results.

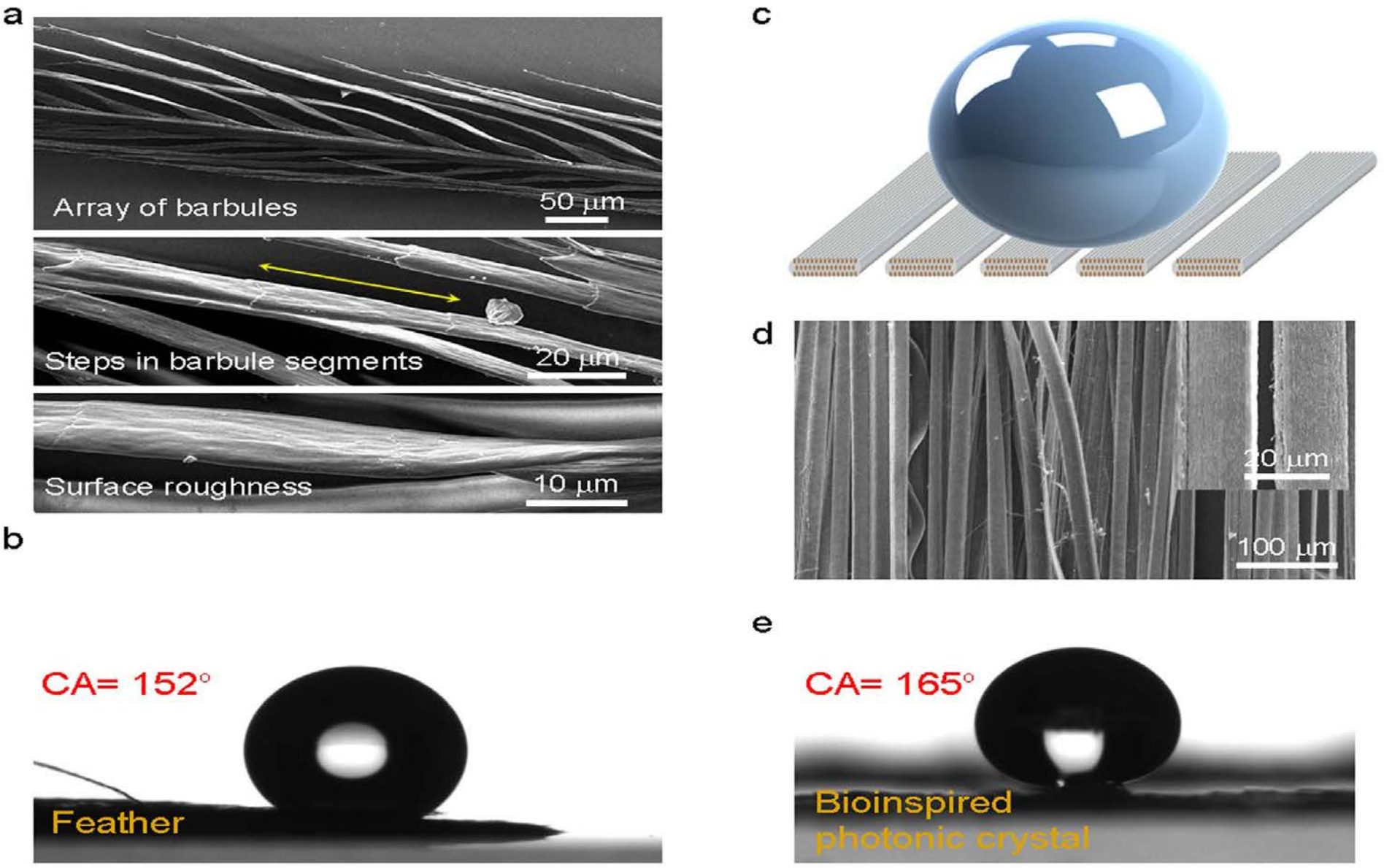

Figure 5 | Enhanced hydrophobicity in feather and feather-inspired photonic crystal structure. (a), Neck feathers exhibit superhydrophobicity due to presence of structural hierarchy. (b), Contact angle measurement of a single mallard feather. (c), Our photonic crystal surface enhances the intrinsic hydrophobicity of PVDF film (see Figure S5) by increasing surface roughnesses. (d), The nanoscale surface pattern observed on step III structures and the alignment of the fiber arrays both contribute to surface superhydrophobicity. (e), The water contact angle is measured to exceed 165° for this particular array.

✓ Biomimetic Magnetic Nanostructures: A Theranostic Platform Targeting Lipid Metabolism and Immune Response in Lymphoma[4]

- B-세포 림프종 세포 (B-cell lymphoma cells)는 B-세포 수용체 (B-cell receptor)에 의해 콜레스테롤이 의존하여 증식 (pro-proliferation)과 생존 신호 (pro-survival signaling)를 유지한다는 연구가 보고됨. 이러한 림프종 세포의 표적화된 콜레스테롤 고갈 (targeted cholesterol depletion of lymphoma cells)은 우수한 치료 전략이라고 알려져 있음.

- 본 연구는 고밀도 지단백질을 생체 모방한 자기나노 구조 (high-density lipoprotein mimicking magnetic nanostructures (HDL-MNSs))를 개발했는데, HDL-MNSs는 high-affinity HDL receptor, scavenger receptor type B1(SR-B1)에 바인딩 할 수 있고 SR-B1 수용체 양성 림프종 (SR-B1 receptor positive lymphoma cell)의 콜레스테롤 플럭스 메커니즘 (cholesterol flux mechanism)을 방해 할 수 있는 자기 나노 구조 (HDL-MNSs)임.

- 또한, MNS 코어는 외부 무선 주파수 필드 (external radio frequency field)에서 열을 발생시키는 목적을 위해 활용 될 수 있으며 MNS의 열 활성화는 antigen presenting cell의 활성화 및 림프구 트래킹을 초래하는 열 충격 단백질 (heat shock proteins)의 발현을 유도함으로써 선천성 및 적응성 항 종양 면역 반응(innate and adaptive antitumor immune responses)을 유발할 수 있음.

- SR-B1 수용체 (SR-B1 receptor)가 phagolysosome formation을 방지하고 HDL-MNS의 cellular uptake와 결합을 중재한다는 것을 입증함. 콜레스테롤 고갈과 열 활성화 특성을 가진 치료제 (combinational therapeutics)는 SR-B1 발현 림프종 세포 (SR-B1 expressing lymphoma cells)에서 치료 효능을 현저히 개선시켰으며 HDL-MNS는 상업적으로 이용 가능한 조영제와 비교하여 자기 공명 영상 (MRI) 하에서 T2 이완 시간 (T2 relaxation time)을 효과적으로 감소시켰고, 진단 이미징로 사용하는데 있어서, SR-B1 receptor에 대한 HDL-MNS의 특이성은 SR-B1 양성 세포와 음성 세포 사이의 음영 이미지 (contrast) 차이를 선명하게 해주었음.

- 세포 특이적 표적화 (cell specific targeting) 효능을 가지고 있는 HDL-MNS는 콜레스테롤을 조절할 수 있고, 항 종양 면역 반응을 조절하는 열 활성화를 유도 할 수 있으며, MRI에서 높은 contrast를 가지고 이미징 할 수 있어 림프종 (lymphoma)에서 유망한 치료적 플랫폼임을 입증하였음.

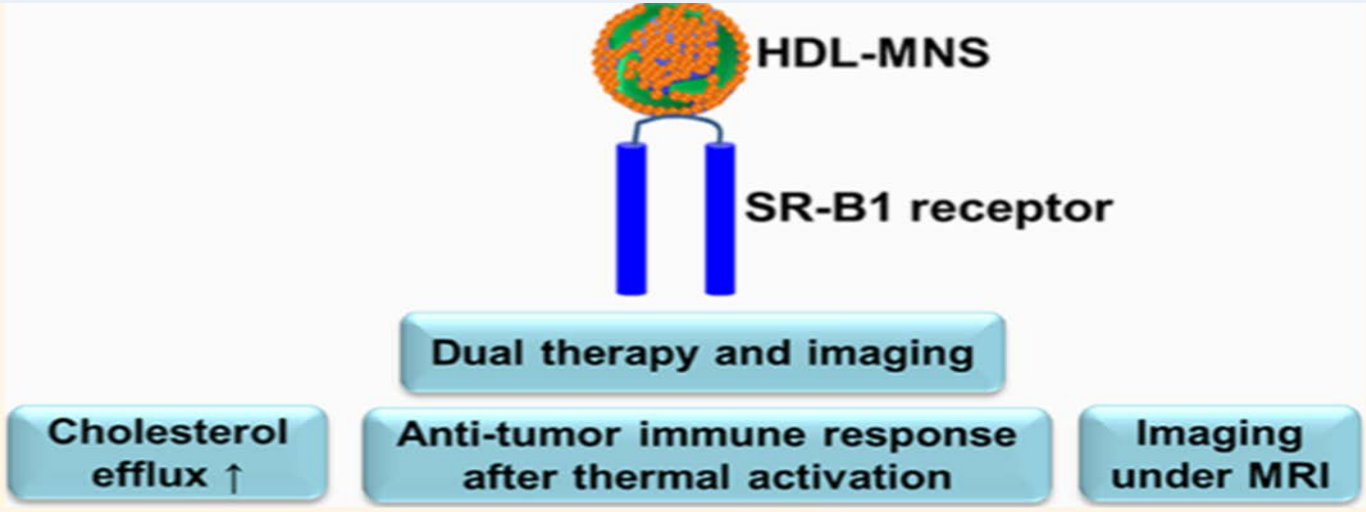

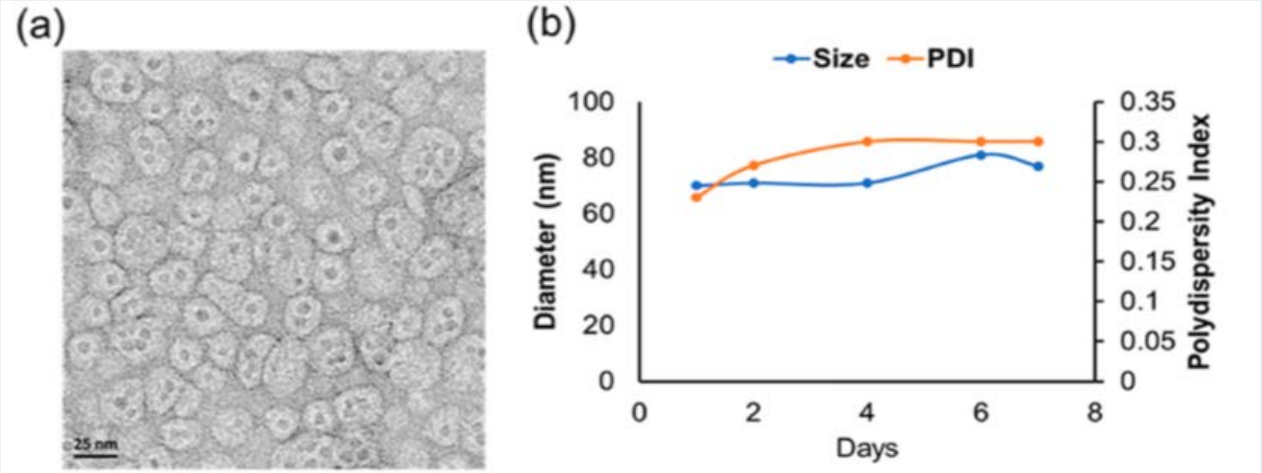

Figure 1. Physicochemical characterization. (a) Transmission electron microscopy image of HDL-MNS. (b) Stability of the HDL-MNS over a week in 10% serum containing media.

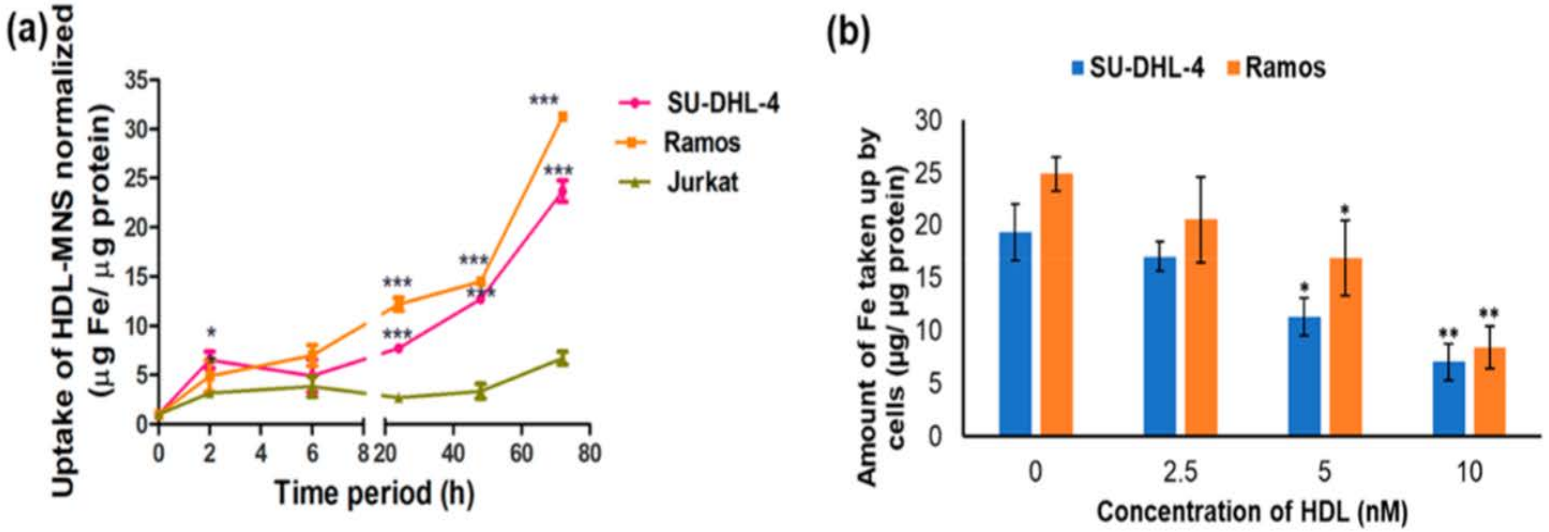

Figure 2. Amount of Fe ion taken up by different cells as measured *via* ICP-MS. (a) A time-dependent study. *$p < 0.05$; **$p < 0.005$; ***$p < 0.0005$, SU-DHL-4 and Ramos *vs* SR-B1 negative Jurkat cells. (b) Receptor binding study to show the uptake of the HDL-MNSs after exposure to natural HDL at 48 h. *$p < 0.05$; **$p < 0.005$; ***$p < 0.0005$, HDL treatment *vs* control cells.

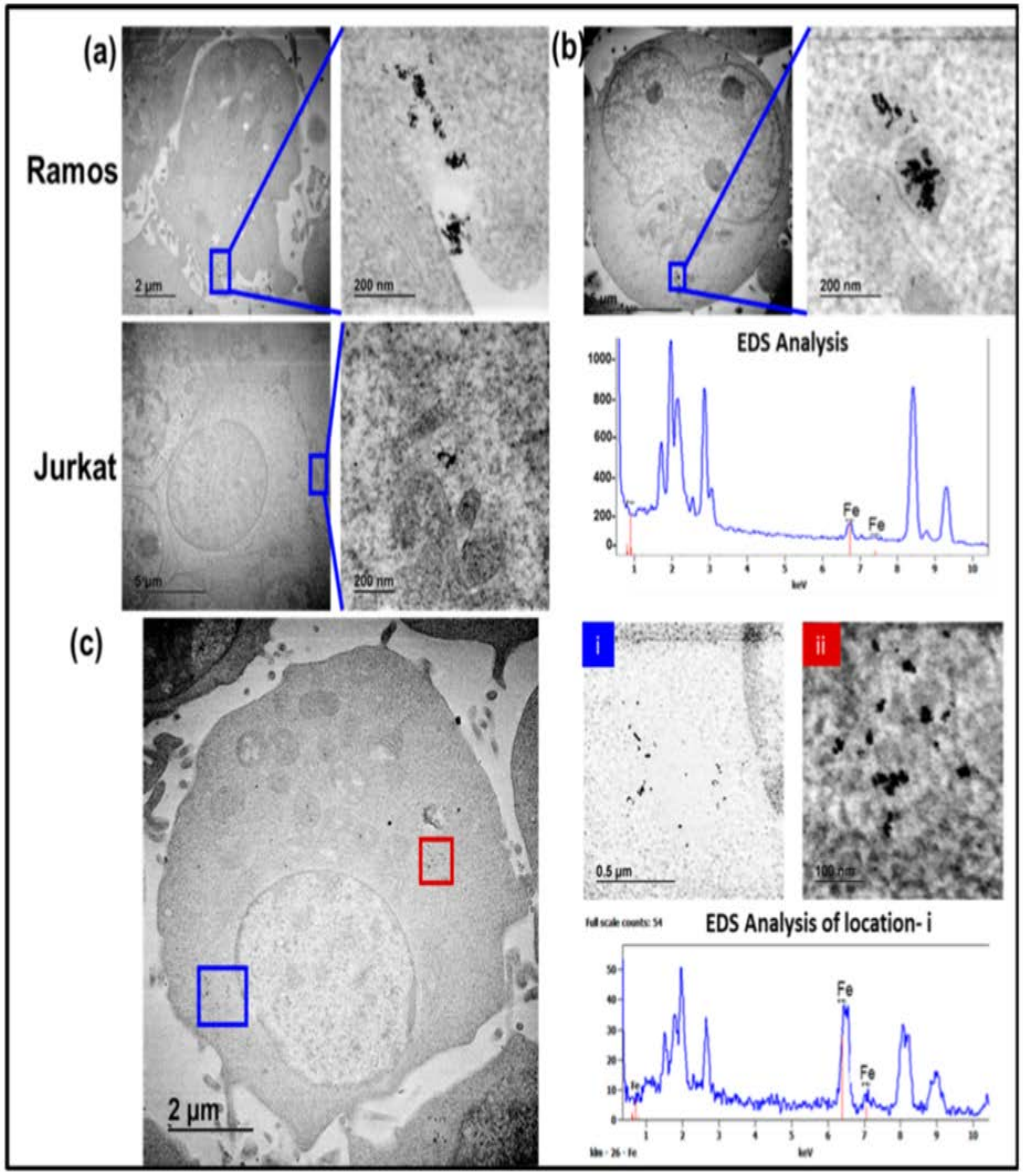

Figure 3. Transmission electron microscopy showing the internalization pattern of the HDL-MNSs in SR-B1 negative (Jurkat) and positive (Ramos) cells. (a) Internalization pattern after 2 h of incubation. (b) Presence of HDL-MNSs in membrane bound vesicles after 24 h of incubation in Jurkat cells and confirmation by EDS analysis. (c) HDL-MNSs are distributed uniformly throughout the Ramos cell after 24 h of incubation. (i) and (ii) are representative images from two parts of the cell. Presence of Fe signal was confirmed by EDS analysis. Additional representative images from both of the cell lines are in Figure S1.

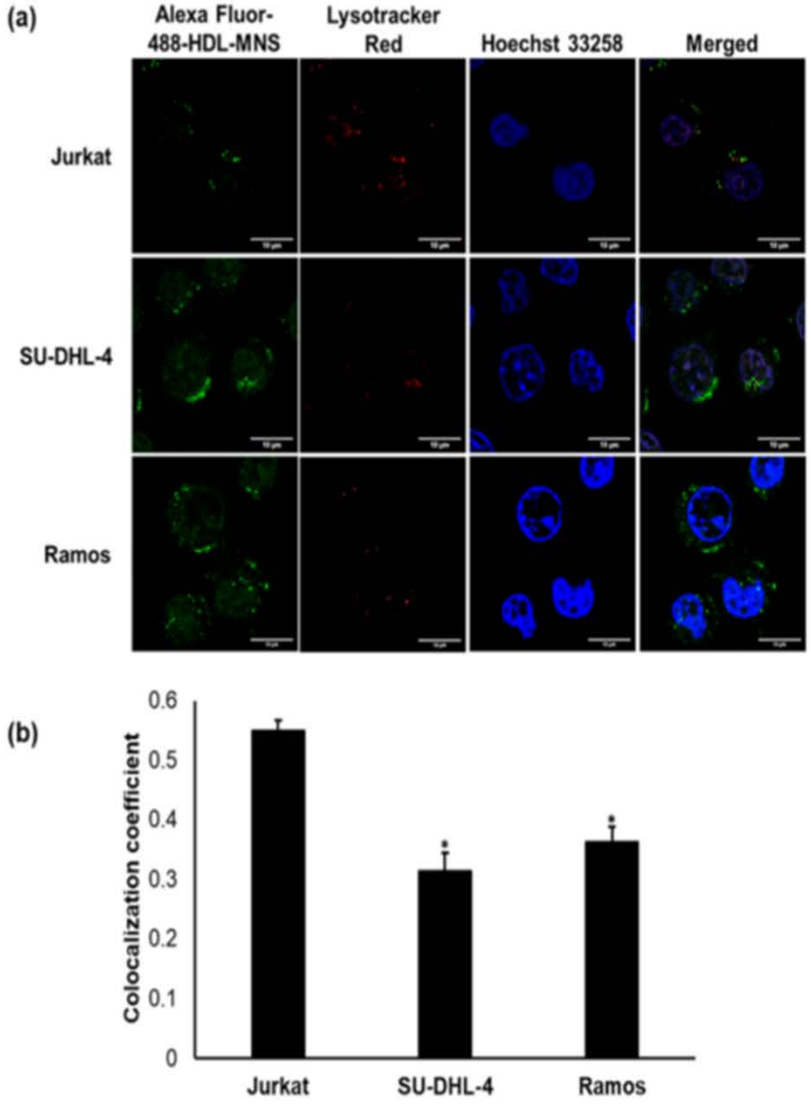

Figure 4. Fluorescence microscopy showing localization of the HDL-MNSs. (a) HDL-MNSs can be observed to be colocalized with lysosome in Jurkat cells and independent of lysosomal vesicles in SR-B1 positive SU-DHL-4 and Ramos cells. (b) Pearson's colocalization coefficient calculated from three different field of views. *$p < 0.05$, SU-DHL-4 and Ramos *vs* SR-B1 negative Jurkat cells.

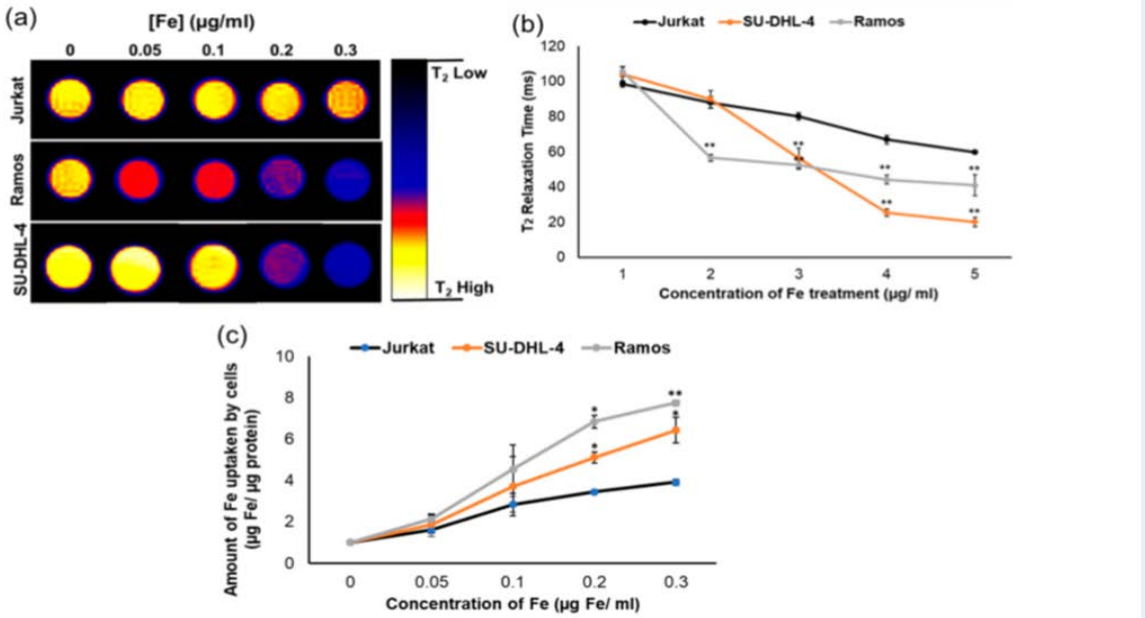

Figure 5. Diagnostic capabilities of the HDL-MNSs. (a) T_2-weighted phantom MRI images. (b) T_2 relaxation times of Jurkat, Ramos, and SU-DHL-4 cell pellets treated with different concentrations of HDL-MNSs using a 7 T Bruker Biospin MRI instrument. (c) Concentration of Fe ion uptaken by different cells at similar concentrations as in the MRI study. The quantification has been done by ICP-MS. *$p < 0.05$, **$p < 0.005$, SR-B1 positive cells *vs* SR-B1 negative Jurkat cells.

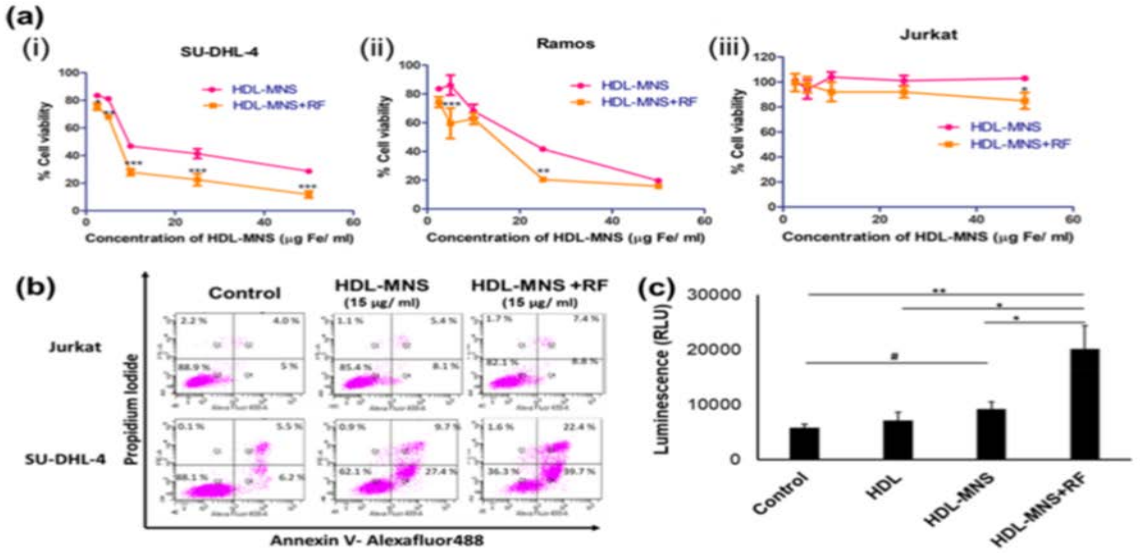

Figure 6. Therapeutic effect of the HDL-MNSs. (a) Cell viability study demonstrating the cytotoxic effect of the HDL-MNSs with and without thermal induction (RF = radiofrequency). *$p < 0.05$; **$p < 0.005$; ***$p < 0.0005$, HDL-MNS treatment *vs* HDL-MNS+RF treatment. (b) Apoptosis study showing the effect of the HDL-MNSs with and without thermal induction on SR-B1 negative Jurkat and SR-B1 positive SU-DHL-4 cell lines. (c) Caspase 3/7 assay in the SR-B1 positive SU-DHL-4 cell line using ApoTox kit. *$p < 0.05$ and **$p < 0.005$, HDL-MNS+RF treatment *vs* other treatment; #$p < 0.05$ HDL-MNS treatment *vs* control.

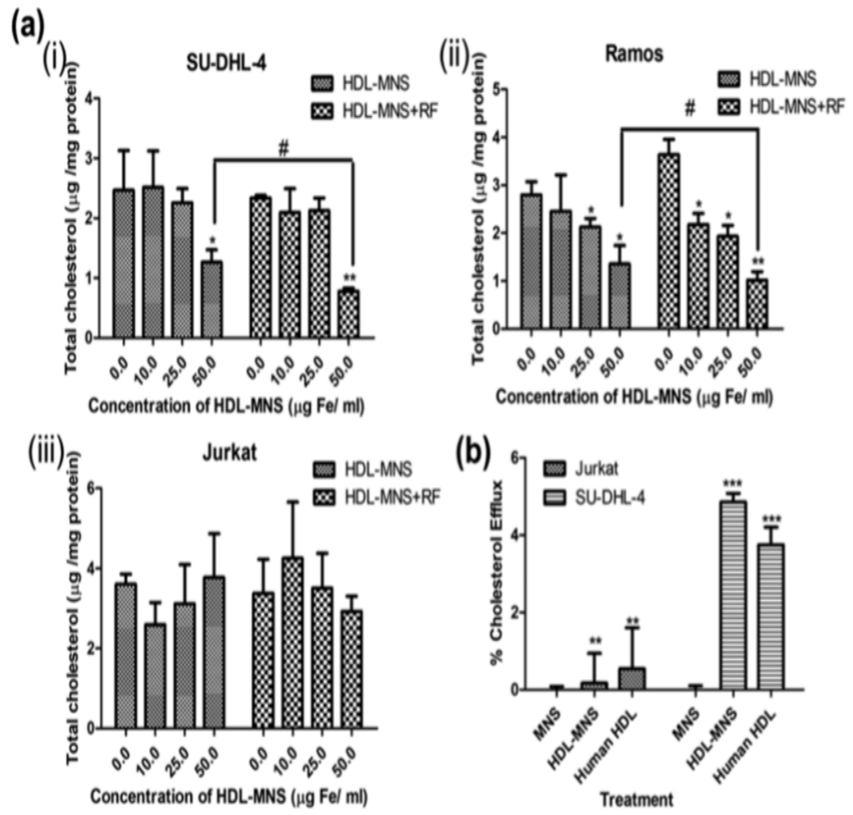

Figure 7. Therapeutic capability of the HDL-MNSs on different lymphoma cell lines. (a) Amount of total cholesterol after treatment with the HDL-MNSs with/without RF. *$p < 0.05$ and **$p < 0.005$, different concentrations of the HDL-MNS treatment *vs* control. #$p < 0.05$, HDL-MNS treatment *vs* HDL-MNS+RF treatment. (b) Cholesterol efflux results showing the role of the HDL-MNSs to efflux the cholesterol out of the different SR-B1 positive and negative lymphoma cells. **$p < 0.005$ and ***$p < 0.0005$, SR-B1 positive cells *vs* SR-B1 negative Jurkat cells.

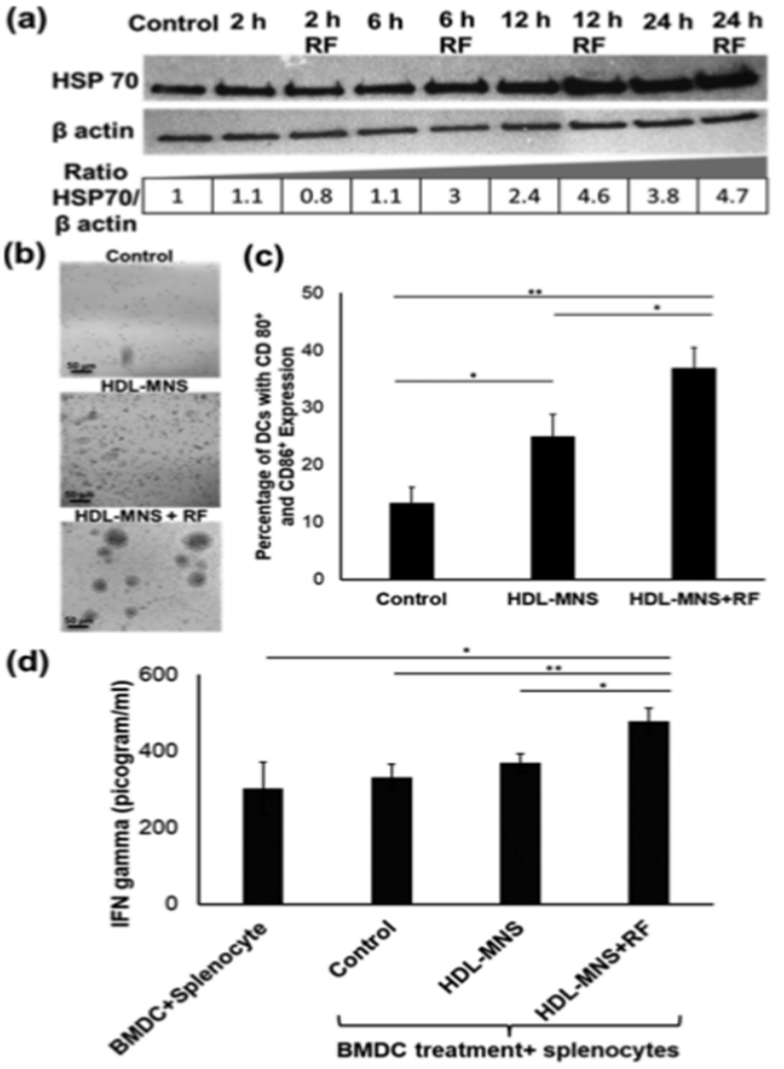

Figure 8. Immunomodulatory responses by the HDL-MNSs after thermal activation. (a) Expression of heat shock protein 70 in SU-DHL-4 cells after treatment with the HDL-MNSs with and without RF induction. (b) Trans-well migration of bone marrow derived dendritic cells toward conditioned media of SU-DHL-4 cells with different treatments. (c) Expression of CD80 and CD86 on dendritic cells exposed to different conditioned media signifying maturation of dendritic cells. *$p < 0.05$ and **$p < 0.005$, control *vs* treatment. (d) ELISA assay showing the release of IFN gamma in the coculture of activated dendritic cells with splenocytes. *$p < 0.05$ and **$p < 0.005$, HDL-MNS+RF *vs* other treatments.

✓ Biomimetic fabrication and photoelectric properties of superhydrophobic ZnO nanostructures on flexible PDMS substrates replicated from rose petal[5]

- Dai et al.은 nanocasting technique을 이용하여 장미 꽃잎 마이크로/나노 구조 (rose petal micro-/nano-structure)를 Polydimethylsiloxane(P은) 로 재현한 결과, 접촉각 (contact angle)이 43°만큼 증가한 153°로 초소수성을 가지게 되었으며, 물방울이 떨어지지 않는 꽃잎 효과 (petal effect)를 확인함.

- 추가적으로 장미 꽃잎이 재현된 P은(rose-petal-like P은)위에 ZnO를 열수 성장 (hydrothermal growth)한 결과, PDMS 표면에 균일한 hexagonal wurtzite structure를 가진 ZnO nanorod가 생성됨. ZnO nanorod의 모양, 높이, 지름 등은 성장 과정에서 성장 시간, 온도, 농도 등의 요소에 의해 결정되었으며 nanorod가 성장된 rose-petal-like PDMS는 접촉각(contact angle)이 164°로 소수성의 특성이 커진 것을 보여주었으나, run-off angle이 5°이하였으며 자가세정 (self-cleaning) 특성을 보임. 이는 표면에 성정한 ZnO nanorod로 nanostructure가 연잎 (lotus leaf)과 비슷하게 되어, ZnO의 성장으로 인해 '꽃잎 효과 (petal effect)'가 '연잎 효과 (lotus effect)'로 변하였기 때문임.

- ZnO가 성장한 rose-petal-like PDMS는 어두울 때는 저항이 크지만, UV를 조사하였을 때 저항이 감소하여 optoelectronic device로서 활용이 가능성을 확인함.

- ZnO nanorod가 서로 접촉한 경우 nanowire로서의 역할을 수행하여 성장 조건에 따라 성능이 향상될 수 있으며, PDMS 자체가 유연하고 micro-/ nano-structure에 의해 소수성과 self-cleaning 특성을 가져 다양한 분야에 활용될 가능성을 가지고 있음.

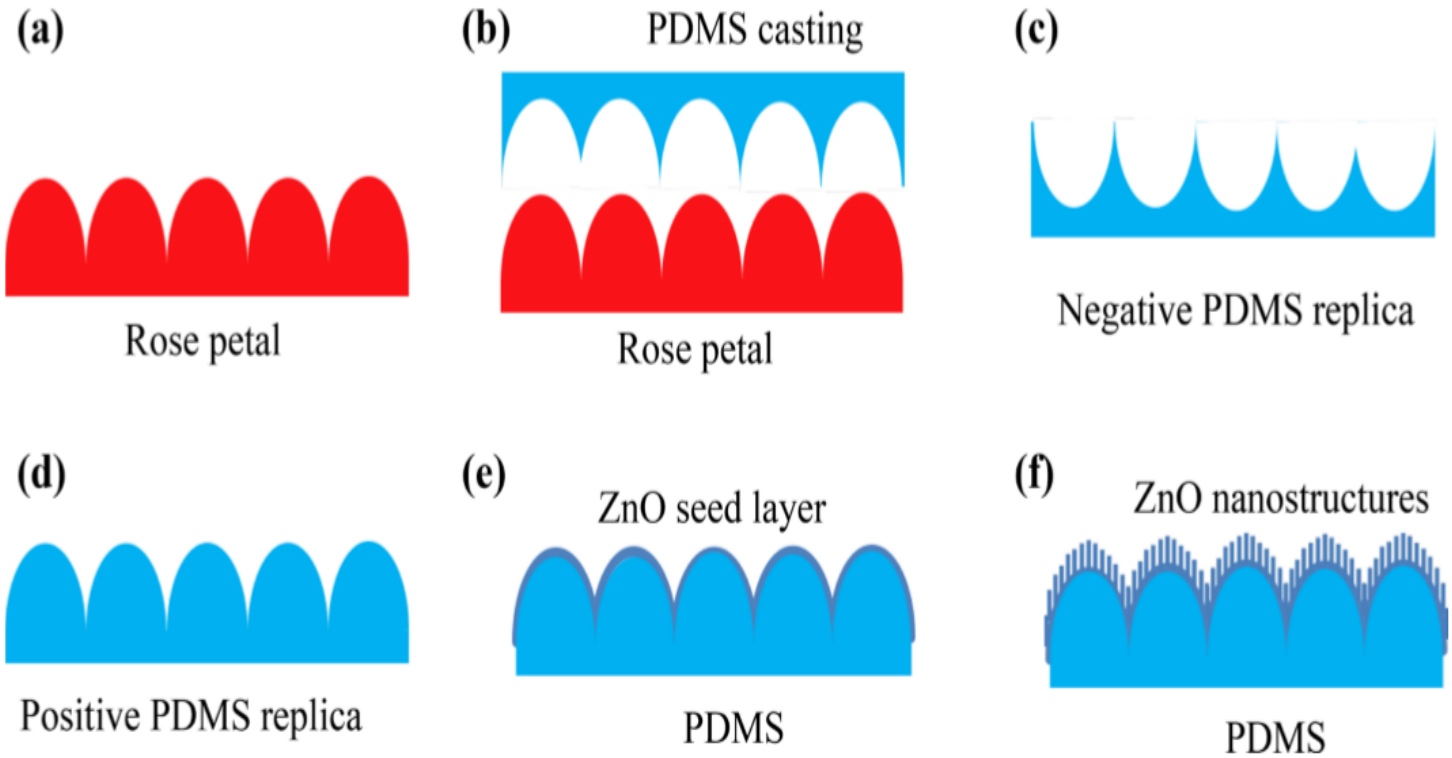

Fig. 1 Schematic representation of the preparation process for the superhydrophobic ZnO nanostructures on PDMS substrates replicated from rose petal. **a** Rose petal, **b** PDMS casting on rose petal, **c** negative PDMS replica peeled off from the rose petal, **d** positive PDMS film replicated from negative PDMS template. **e** Thermal evaporation of ZnO seed layer on PDMS, **f** hydrothermal growth of ZnO nanostructures on PDMS substrate

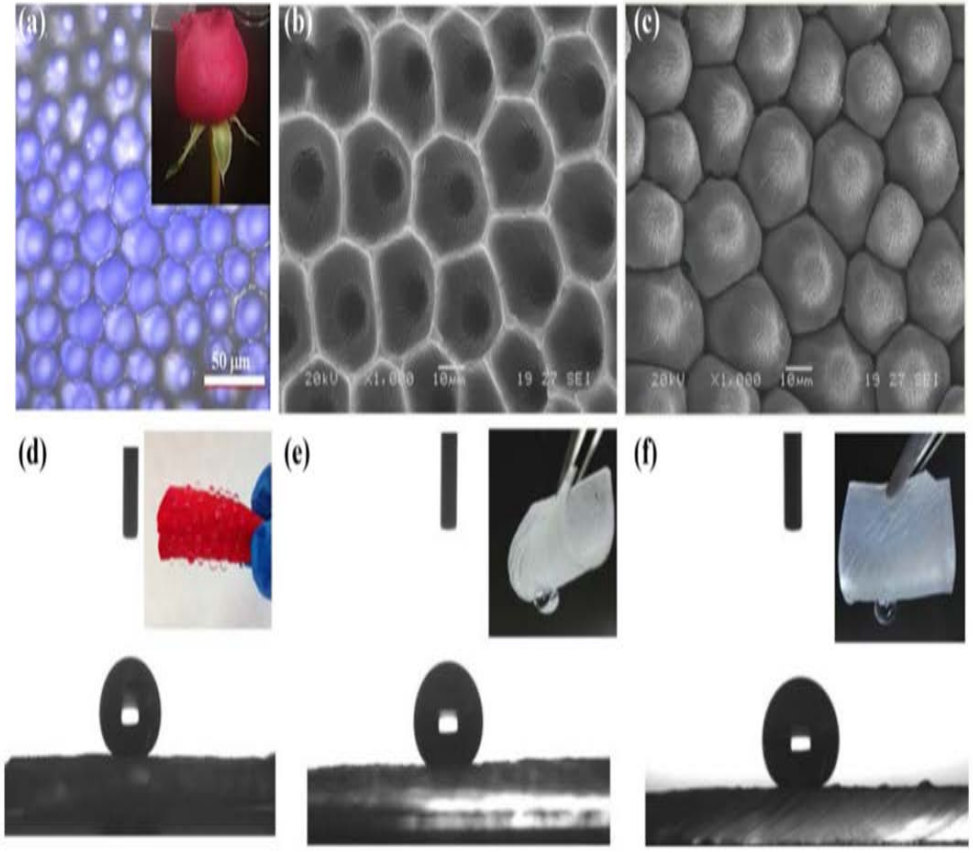

Fig. 2 **a** Optical image of fresh rose petal, SEM images of **b** negative and **c** positive PDMS replicas. CA measurements of **d** fresh rose petal, **e** negative and **f** positive PDMS replicas

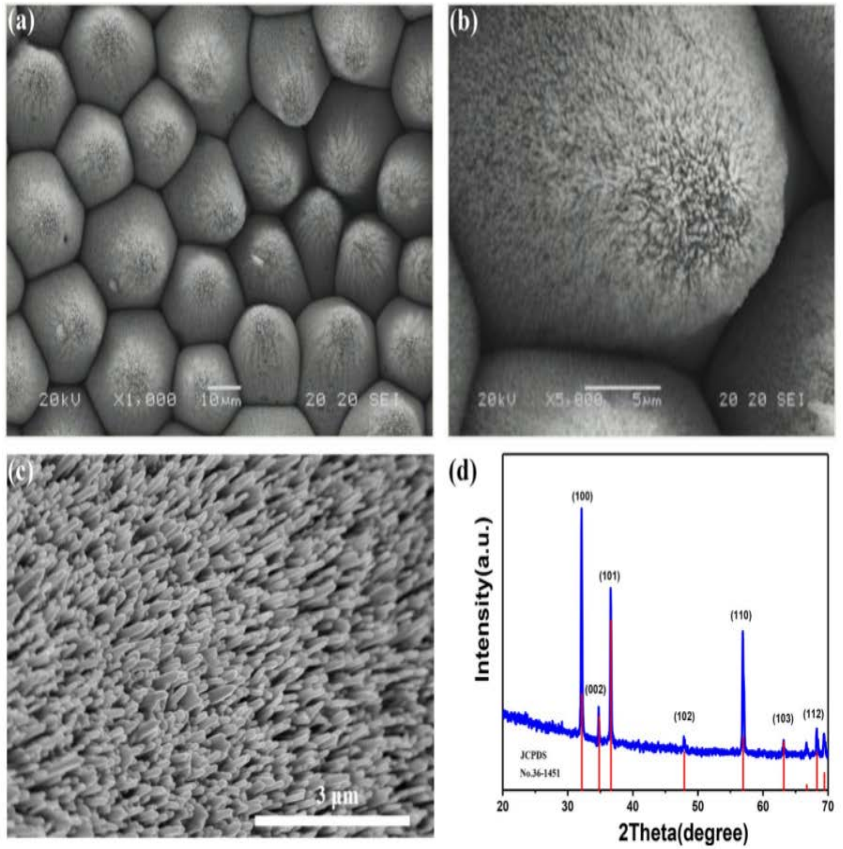

Fig. 3 **a, b** SEM, **c** FESEM and HRTEM images and **d** XRD pattern of typical ZnO nanostructures grown on the rose-petal-like PDMS substrate after hydrothermal growth for 8 h with $Zn(NO_3)_2$ concentrations of 25 mM

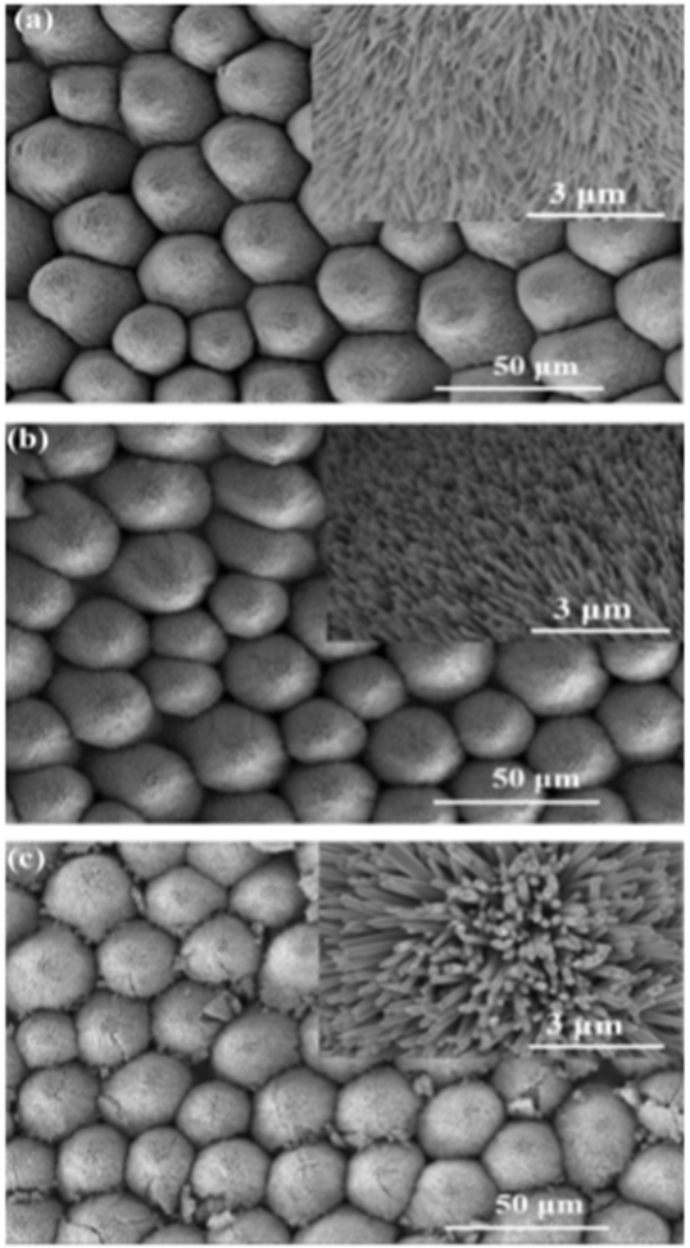

Fig. 4 SEM images of ZnO nanostructures grown on the rose-petal-like PDMS substrate after hydrothermal growth for 8 h with $Zn(NO_3)_2$ concentrations of **a** 10, **b** 25, and **c** 50 mM, respectively (Scale bar = 3 μm). Insets: high-magnified FESEM images of ZnO nanostructures obtained on the PDMS micropillars (Scale bar = 3 μm)

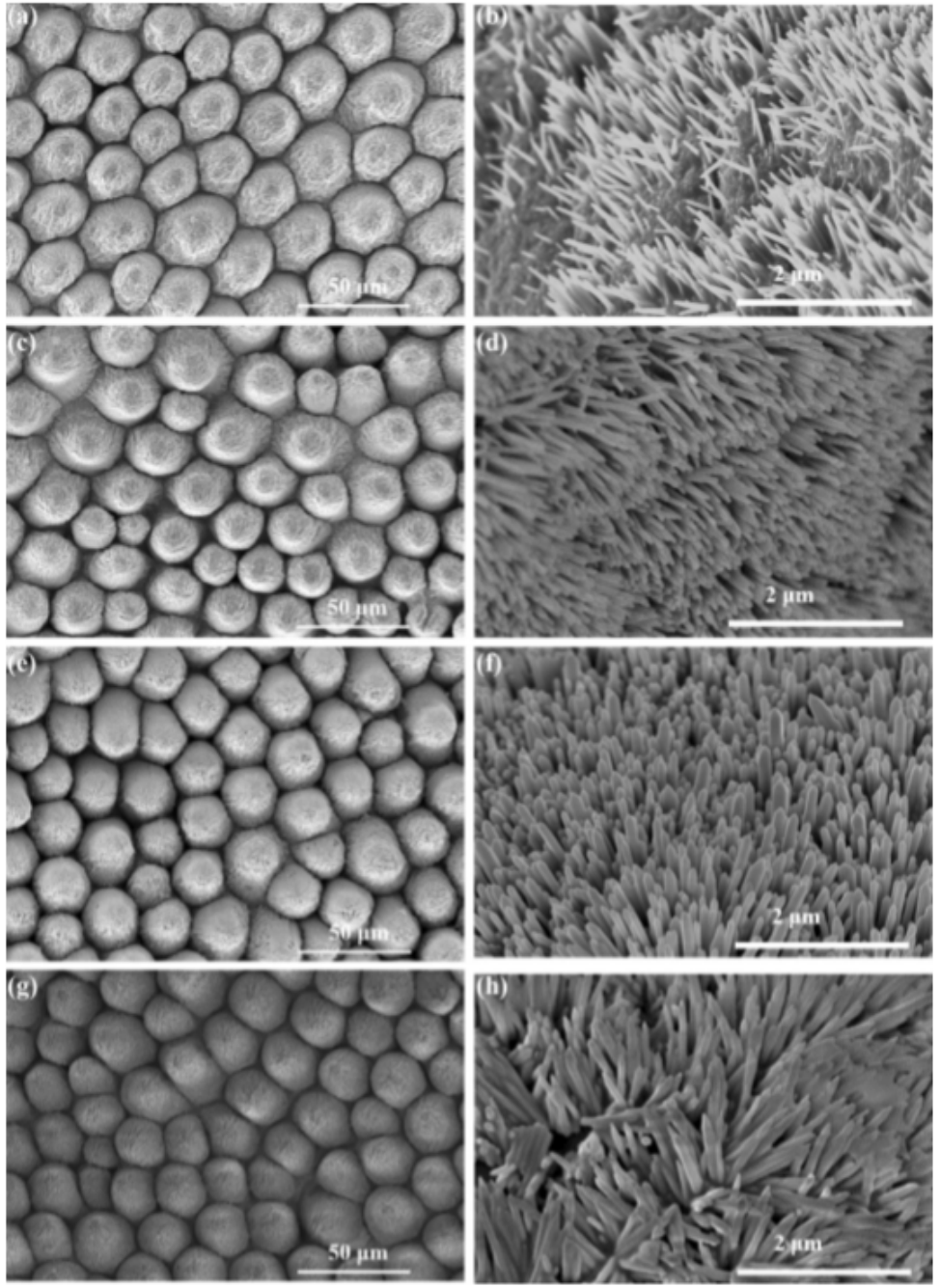

Fig. 5 SEM images of ZnO nanostructures on the rose-petal-like PDMS substrate after hydrothermal growth with 25 mM $Zn(NO_3)_2$ for **a, b** 1 h, **c, d** 2 h, **e, f** 4 h, and **g, h** 12 h, respectively. (Scale bar = 50 μm for **a, c, e, g** and scale bar = 2 μm for **b, d, f, h**)

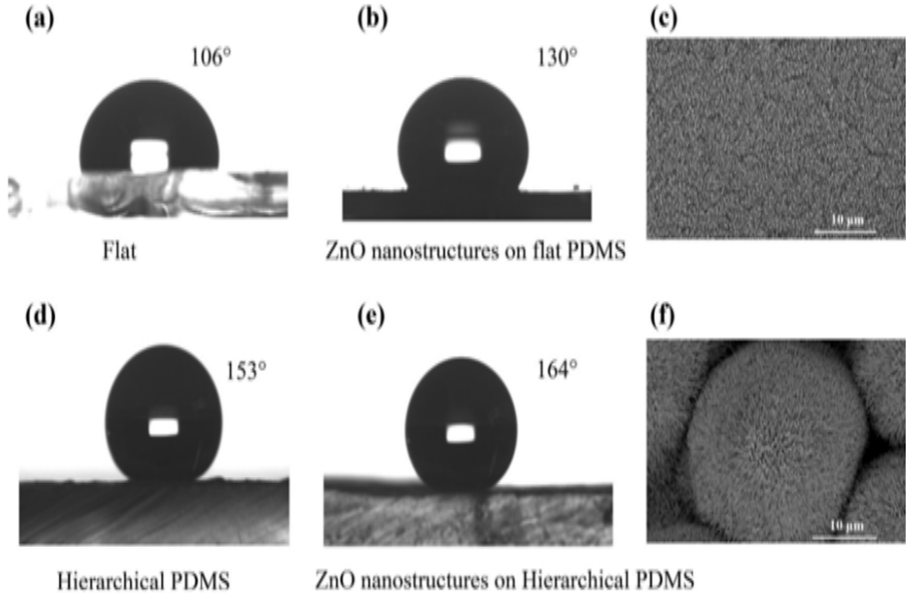

Fig. 6 CA **a** of flat PDMS film. CA **b** and SEM image **c** of ZnO nanorod arrays on flat PDMS. CA **d** of rose-petal-like PDMS. CA **e** and SEM image **f** of ZnO/PDMS hierarchical structures. The ZnO nanostructures were obtained after hydrothermal growth with 25 mM $Zn(NO_3)_2$ for 8 h. (Scale bar = 10 μm)

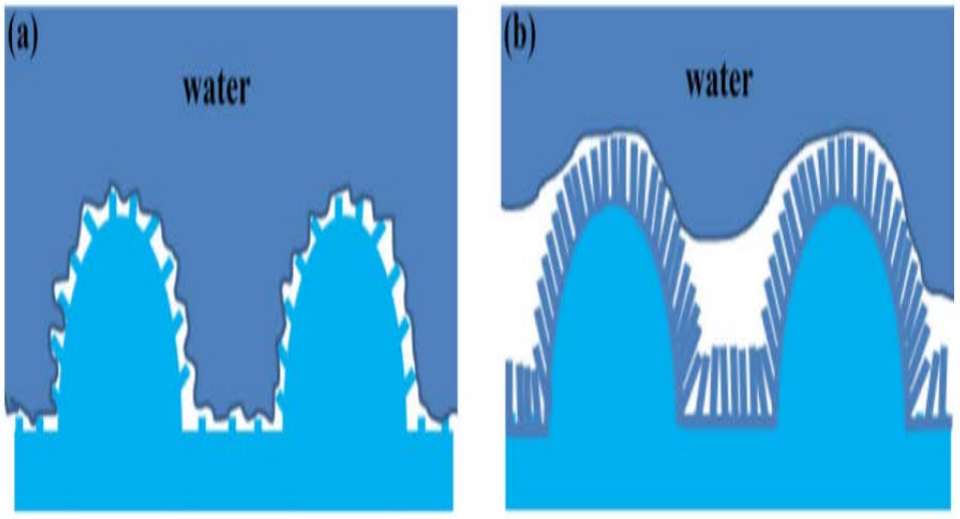

Fig. 7 Schematic representations of contact modes of a drop of water with **a** rose-petal-like PDMS and **b** ZnO/PDMS hierarchical structures

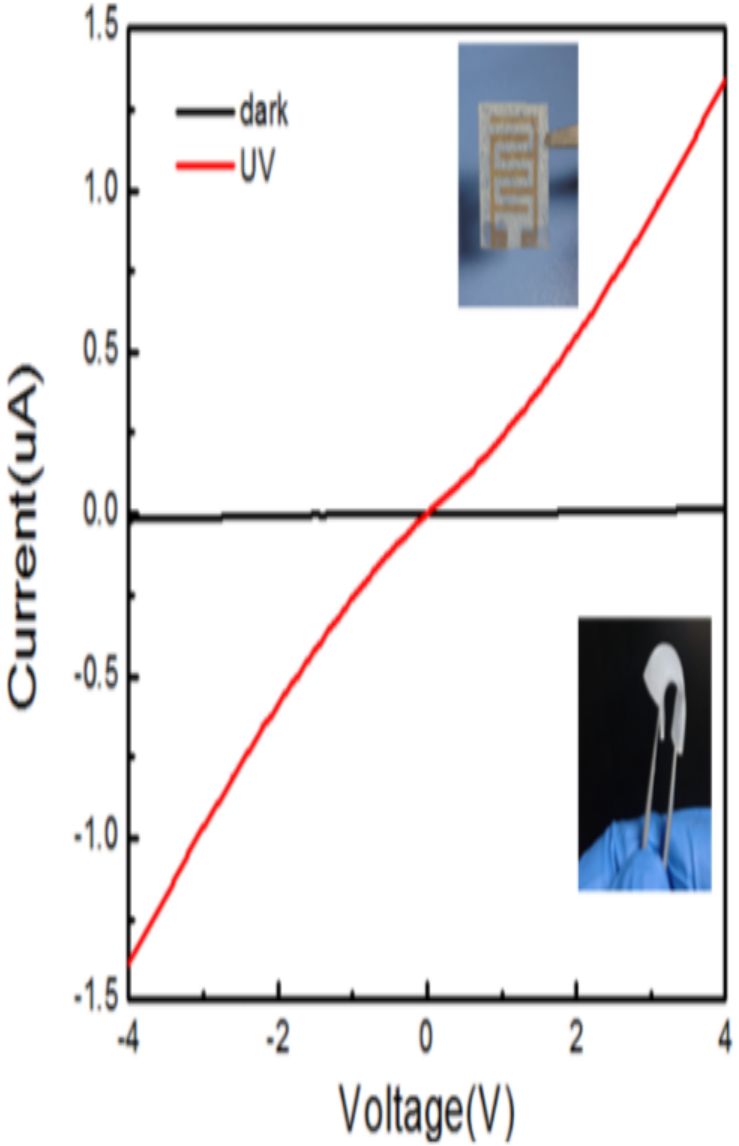

Fig. 8 Typical dark and UV illuminated I–V characteristics of ZnO/PDMS hierarchical micro/nano structures. Insets: optical images of the device based on ZnO/PDMS hierarchical surface

참고 문헌

1. Biomimetic fabrication of micro-/nanostructure on polypropylene surfaces with high dynamic superhydrophobic stability, Han-Xiong Huang∗, Xue Wang, Materials Today Communications, 19, 2019

2. Biomimetic Nanostructure Fabrication to Increase Light Transmission Efficiency in Optoelectronic Devices, P. Sotory and A. Bozkurt, IEEE SENSORS, 2019

3. Biomimicry of multifunctional nanostructures in the neck feathers of mallard (Anas platyrhynchos L.) drakes, T. Khudiyev, T. Dogan and M. Bayindir, SCIENTIFIC REPORTS, 4, 2014

4. Biomimetic Magnetic Nanostructures: A Theranostic Platform Targeting Lipid Metabolism and Immune Response in Lymphoma, A.Singh, V. Nandwana, J. S. Rink, S.-R. Ryoo, T. H. Chen, S. D. Allen, E. A. Scott, L. I. Gordon, C. S. Thaxton, and V. P. Dravid,*acs Nano, 13, 2019

5. **Biomimetic fabrication and photoelectric properties of superhydrophobic ZnO nanostructures on flexible PDMS substrates replicated from rose petal, S. Dai, Y. Zhu, Y. Gu, Z. Du, Applied Physics A, 125, 2019**